

PHYTOCHROME C plays a major role in the acceleration of wheat flowering under long-day photoperiod

Andrew Chen^{a,1}, Chengxia Li^{a,b,1}, Wei Hu^{c,1}, Mei Yee Lau^a, Huiqiong Lin^a, Nathan C. Rockwell^c, Shelley S. Martin^c, Judith A. Jernstedt^a, J. Clark Lagarias^{c,2}, and Jorge Dubcovsky^{a,b,2}

Departments of ^aPlant Sciences and ^cMolecular and Cellular Biology, University of California, Davis, CA 95616; and ^bHoward Hughes Medical Institute, Chevy Chase, MD 20815

This contribution is part of the special series of Inaugural Articles by members of the National Academy of Sciences elected in 2013.

Contributed by Jorge Dubcovsky, May 30, 2014 (sent for review March 9, 2014; reviewed by Ben Trevaskis and Jorge J. Casal)

Phytochromes are dimeric proteins that function as red and far-red light sensors influencing nearly every phase of the plant life cycle. Of the three major phytochrome families found in flowering plants, PHYTOCHROME C (PHYC) is the least understood. In *Arabidopsis* and rice, PHYC is unstable and functionally inactive unless it heterodimerizes with another phytochrome. However, when expressed in an *Arabidopsis phy*-null mutant, wheat PHYC forms signaling active homodimers that translocate into the nucleus in red light to mediate photomorphogenic responses. Tetraploid wheat plants homozygous for loss-of-function mutations in all PHYC copies (*phyC^{AB}*) flower on average 108 d later than wild-type plants under long days but only 19 d later under short days, indicating a strong interaction between PHYC and photoperiod. This interaction is further supported by the drastic down-regulation in the *phyC^{AB}* mutant of the central photoperiod gene *PHOTOPERIOD 1* (*PPD1*) and its downstream target *FLOWERING LOCUS T1*, which are required for the promotion of flowering under long days. These results implicate light-dependent, PHYC-mediated activation of *PPD1* expression in the acceleration of wheat flowering under inductive long days. Plants homozygous for the *phyC^{AB}* mutations also show altered profiles of circadian clock and clock-output genes, which may also contribute to the observed differences in heading time. Our results highlight important differences in the photoperiod pathways of the temperate grasses with those of well-studied model plant species.

development | flowering time | temperate cereals | TILLING | ethyl methane sulphonate

Plants use several families of photoreceptors, including phytochromes, to optimize growth and development under different light environments. Plant phytochromes are dimeric proteins with covalently bound linear tetrapyrrole (bilin) chromophores that function as red/far-red photoreceptors (1). Phytochromes are synthesized in a biologically inactive red light-absorbing form (Pr) that is photoconverted into the biologically active far red-absorbing form (Pfr) upon exposure to red light. Exposure to far-red wavelengths reverses Pfr to Pr, resulting in a dynamic equilibrium in changing light environments. Phytochromes translocate into the nucleus following conversion to Pfr, where they regulate transcriptional signaling networks (2–5). Phytochromes also perform cytoplasmic regulatory roles that are less understood (6).

Phytochromes are encoded by three genes (*PHYA*, *PHYB*, and *PHYC*) in most monocot species whereas eudicot plant species possess additional genes (*PHYD-F*) derived from *PHYB* duplications (7, 8). Studies in model plant species have shown that *PHYA* is required for growth in deep shade and for seedling deetiolation (9) whereas members of the *PHYB* clade play major roles in shade-avoidance responses (10, 11). Genetic studies implicate PHYC in regulatory functions during early seedling development and in shade-avoidance responses in both *Arabidopsis* and rice (12, 13). Because *phyC* mutants of both species

flower 2–3 wk earlier than wild type under noninductive photoperiods [i.e., short days (SD) for *Arabidopsis* and long days (LD) for rice] (13, 14), PHYC appears to function as a flowering repressor under noninductive photoperiods in these two species.

In wheat and barley, the chromosome region encompassing *PHYC* has been associated with differences in flowering time under inductive LD photoperiods, but genetically linked loci have not been ruled out as candidate flowering time genes (15–18). In both species, *PHYC* is tightly linked to the *VERNALIZATION 1* (*VRN1*) gene, a MADS-box meristem identity gene similar to *Arabidopsis APETALA1*, which promotes the vegetative-to-reproductive transition of the shoot apical meristem (19–21). A deletion encompassing *PHYC*, *VRN1*, and other linked genes was previously detected in a nonflowering radiation mutant in diploid wheat (*Triticum monococcum* L.), designated *maintained vegetative phase* (*mvp*) (15, 18). The inability of this mutant to flower was initially attributed to the deletion of *VRN1* (15, 22). However, a recent study of *vm1* knockout mutants in tetraploid wheat established that *VRN1* is not essential for wheat flowering (21),

Significance

Plants perceive day length as a critical environmental signal to trigger major changes in development. Multiple light sensors participate in day-length perception, the most important of which are the red/far-red phytochromes. In rice and *Arabidopsis*, PHYTOCHROME C (PHYC) requires other phytochromes for stability and function. By contrast, wheat PHYC is stable and functionally active even in the absence of other phytochromes. The loss of functional wheat PHYC results in altered expression of circadian clock and photoperiod genes and a dramatic delay in flowering under long days, indicating that PHYC promotes wheat flowering under inductive photoperiods. Our results provide an additional entry point to modify wheat flowering and to accelerate the development of wheat varieties better adapted to new and changing environments.

Author contributions: A.C., C.L., W.H., J.C.L., and J.D. designed research; A.C., C.L., W.H., M.Y.L., H.L., N.C.R., S.S.M., and J.A.J. performed research; A.C., C.L., W.H., J.C.L., and J.D. analyzed data; A.C., C.L., W.H., J.C.L., and J.D. wrote the paper; M.Y.L., H.L., N.C.R., S.S.M., and J.A.J. contributed to revision of the manuscript; and J.D. wrote initial and final versions of the manuscript.

Reviewers: B.T., Commonwealth Scientific and Industrial Research Organization; and J.J.C., Universidad de Buenos Aires.

The authors declare no conflict of interest.

Freely available online through the PNAS open access option.

Data deposition: The sequences reported in this paper have been deposited in the GenBank database (accession nos. [KF859916](#) and [KF859917](#)).

See Profile 10.1073/pnas.1410244111.

¹A.C., C.L., and W.H. contributed equally to this work.

²To whom correspondence may be addressed. E-mail: jdubcovsky@ucdavis.edu or jclagarias@ucdavis.edu.

This article contains supporting information online at www.pnas.org/lookup/suppl/doi:10.1073/pnas.1409795111/-DCSupplemental.

raising the possibility that the *PHYC* deletion is responsible for the nonflowering phenotype of the *mvp* mutant.

Phenotypic data of *phyC* mutants do not distinguish between “direct” or “indirect” roles of PHYC to modulate activities of other phytochromes. Indeed, PHYC is unstable in the absence of PHYB clade members with which it heterodimerizes in both model plant species *Arabidopsis* and rice (13, 23). We show here that wheat PHYC not only can form homodimers that translocate into nuclei of transgenic *phy*-null *Arabidopsis* seedlings (24), but also can mediate photomorphogenic responses in the absence of other phytochromes. We also establish that *PHYC* is required for acceleration of wheat flowering under inductive LD, a response mediated by light-dependent activation of the photoperiod gene *PHOTOPERIOD 1* (*PPD1*) and its downstream target *FLOWERING LOCUS T1* (*FT1*) (25). Wheat *FT1* is a homolog of *Arabidopsis FT* and rice *HD3A* genes, which encode mobile proteins critical for the transmission of day-length signals from leaves to the shoot apical meristem (26, 27). Our studies also reveal a regulatory role of wheat PHYC on the circadian clock, which highlights the differences between the photoperiod sensing pathways of the temperate grass species and those of the two best-known model plant species.

Results

Loss-of-Function Mutations for *PHYC* Have a Strong Effect on Wheat Flowering. The tetraploid wheat variety Kronos (*Triticum turgidum* L., $2n = 28$, genomes AABB) used in this study has a spring growth habit (*Vrn-A1c* allele) and shows accelerated flowering under LD photoperiods (*Ppd-A1a* allele) (*Materials and Methods*). We obtained full-length genomic sequences of both *PHYC* homeologs (*PHYC^A* = KF859916 and *PHYC^B* = KF859917) from Kronos, using primers described in *SI Appendix, Table S1*, and then developed genome-specific primers (*SI Appendix, Table S2*) to screen a Kronos mutant population (28). We identified 42 mutations resulting either in truncations or amino acid changes in both A- and B-genome copies of *PHYC* (*SI Appendix, Table S3*). Mutant T4-2327 for the A genome copy (henceforth, *phyC^A*) and mutant T4-807 for the B genome copy

(henceforth, *phyC^B*) were selected for the present study (*SI Appendix, Table S3*).

The selected *phyC^A* mutation disrupts the donor splice site at the end of exon 2 and generates a premature stop codon. The protein encoded by this mutant is predicted to lack the last 179 amino acids of the C-terminal region (Fig. 1A) known to be critical for phytochrome dimerization (23, 29). The truncated *PHYC^A* protein does not form homodimers in yeast two-hybrid assays (*SI Appendix, Fig. S1A*) nor could be detected by immunoblot analysis (*SI Appendix, Fig. S1B*), implying its instability in vivo. The selected *phyC^B* mutant encodes a protein with a substitution of a cysteine (“C”) residue in the GAF domain (C323Y) (Fig. 1A) that is required for bilin chromophore binding (1). We confirmed that the protein encoded by the *phyC^B* mutant allele is not photoactive (*SI Appendix, Fig. S1C*) using an *Escherichia coli* system engineered for coproduction of its phytochromobilin (PΦB) chromophore (30).

Under inductive LD photoperiods, plants homozygous for the *phyC^A* mutation flower at the same time as wild-type Kronos whereas those homozygous for the *phyC^B* mutation flower 8 d later ($P < 0.0001$) (Fig. 1B). The larger effect of the *phyC^B* mutation relative to the *phyC^A* mutation may be associated with the higher *PHYC^B* transcript accumulation relative to *PHYC^A* (*SI Appendix, Fig. S2A* and primers in *SI Appendix, Table S5*), but we cannot rule out the possibility that the substitutions of conserved amino acids observed only in *PHYC^B* (*SI Appendix, Table S4*) may also contribute to its stronger effect on heading time. Wheat plants homozygous for either *phyC^A* or *phyC^B* mutations exhibit normal spike and flower morphology and fertility. By contrast, plants homozygous for both mutations (henceforth *phyC^{AB}*) show altered spike and spikelet development, reduced grain set, and elongated rachises, glumes, and glume awns (*SI Appendix, Fig. S3* and *Table S6*). Seedlings carrying the *phyC^{AB}* mutations show a significant increase in coleoptile length under red light (~10% increase, $P = 0.0002$) (*SI Appendix, Table S7*), indicating a mild impairment in red light-mediated photomorphogenesis. No significant differences in coleoptile length between these two alleles were detected in the dark or under continuous blue or far red light (*SI Appendix, Table S7*).

More importantly, flowering of the *phyC^{AB}* mutant is dramatically delayed under inductive LD photoperiods (average 108 d, $P < 0.0001$) (Fig. 1C and D). Flowering is also delayed under noninductive SD, but the effect is fivefold smaller than under LD (average 19 d, $P < 0.0001$) (Fig. 1D), suggesting the existence of an interaction between *PHYC* and photoperiod on heading time. The significance of this interaction was confirmed in a factorial ANOVA ($P < 0.0001$). Interestingly, the *phyC^{AB}* mutant flowered 18 d earlier under SD than under LD (Fig. 1D), suggesting that, at least for this particular genotype (*Ppd-A1a* allele), wheat plants with nonfunctional *PHYC* alleles behave like an SD plant.

Wheat PHYC Protein Can Form Homodimers and Restore Photomorphogenic Responses in an *Arabidopsis phy*-Null Mutant. The strong effect of the wheat *phyC^{AB}* mutants on flowering time relative to the milder effects of *phyC* mutants in *Arabidopsis* and rice prompted us to examine wheat PHYC using biochemical approaches. In *Arabidopsis* and rice, PHYC function requires the presence of PHYB-clade members because the PHYC protein is degraded in their absence (13, 14, 23, 24). Yeast two-hybrid assays show that wheat PHYC can form heterodimers with wheat PHYB (*SI Appendix, Fig. S4A*), an interaction previously shown in *Arabidopsis* and rice. Unexpectedly, wheat PHYC also can form homodimers, an interaction not observed when *Arabidopsis* PHYC is used as control (Fig. 2A and primers in *SI Appendix, Table S8*). The C terminus of the wheat PHYC protein shows the strongest homodimeric interaction (Fig. 2A), consistent with the known role of the C-terminal region in phytochrome

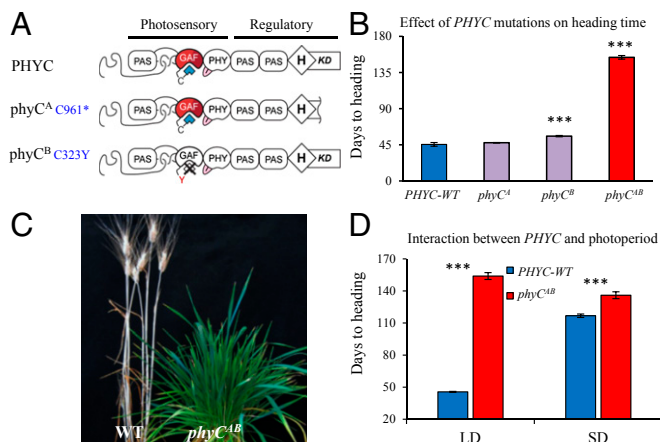


Fig. 1. Characterization of *phyC* mutants. (A) Diagrammatic representation of the wild-type and mutant PHYC proteins. The blue polygon represents the chromophore binding to the GAF domain, except for the *PHYC^B* mutant C323Y. (B) Heading time of wild type and single and double *phyC* mutants grown under LD. (C) Representative wild-type and *phyC^{AB}* tetraploid wheat plants grown for 15 wk under LD. (D) Differential effect of *PHYC* on heading time under short (SD) and long days (LD). Error bars represent SEMs based on eight plants. *** $P < 0.001$, based on Dunnett's test comparing each mutant to wild type in B and on tests for simple effects of *PHYC* within photoperiod in a factorial ANOVA in D.

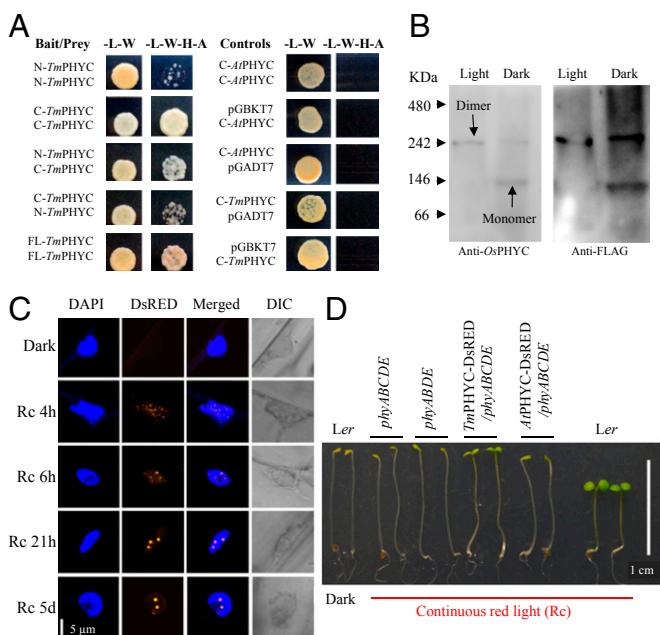


Fig. 2. Wheat PHYC function is observed even in the absence of other phytochromes. (A) Yeast two-hybrid assays. (Left) Pairwise interactions between full-length wheat PHYC protein from *T. monococcum* (FL-*TmPHYC*), and both N-terminal (N-*TmPHYC*) and C-terminal truncations (C-*TmPHYC*). Synthetic dextrose minimal medium lacking Leucine and Tryptophan (–L–W) was used to select for yeast transformants containing both bait and prey vectors. Interaction strength was tested on the same medium lacking Leucine, Tryptophan, Histidine, and Adenine (–L–W–H–A). Note the strong homodimeric interaction of the C-terminal truncation, which is consistent with the known role of the C-terminal region in phytochrome dimerization (23). (Right) Homodimerization tests for *Arabidopsis* PHYC (*AtPHYC*) and autoactivation tests for *AtPHYC* and *TmPHYC*. (B) Native immunoblots of proteins extracted from seedlings of *Arabidopsis phyABCDE*-null mutant transformed with *TmPHYC*-FLAG grown under continuous light or in the dark. (C) Confocal fluorescence microscopy of *Arabidopsis phyABCDE* lines transformed with *TmPHYC*-DsRED grown in the dark for 5 d and then exposed to continuous red light. DAPI (4',6-diamidino-2-phenylindole) was used to stain cell nuclei and differential interference contrast (DIC) to show position of the nuclei in the cell. (D) Wild-type *Ler* plants grown in the dark compared with 5-d-old *Ler* and *phy* mutant plants grown under continuous red light ($50 \mu\text{mol}\cdot\text{m}^{-2}\cdot\text{s}^{-1}$). *Arabidopsis phyABDE* has a wild-type *PHYC*. *Arabidopsis phyABCDE* was transformed with either *TmPHYC*-DsRED or *AtPHYC*-DsRED as control.

dimerization (23, 29). Using split luciferase assays in rice protoplasts, we also observed that wheat PHYC is able to form homodimers (SI Appendix, Fig. S4B). Although the presence of *PHYC* homodimers in wheat plants has not been confirmed, the higher transcript level of *PHYC* relative to *PHYB* (SI Appendix, Fig. S5) (10-fold difference) suggests a good probability for the presence of such homodimers in wheat plants.

We next examined the ability of wheat PHYC to form homodimers in planta by constitutive expression of a transgene encoding a FLAG-tagged *T. monococcum* PHYC (*TmPHYC*-FLAG) (SI Appendix, Table S9) in an *Arabidopsis phyABCDE* mutant lacking all phytochromes (24). Native immunoblot analysis of soluble protein extracts from these transgenic plants grown under continuous light reveals a 260-kDa band consistent with a *TmPHYC*-FLAG dimer (Fig. 2B). By comparison, both monomer and dimer forms of *TmPHYC* are detected in protein extracts of dark-grown seedlings (Fig. 2B). These observations suggest that *TmPHYC* dimer formation and/or *TmPHYC* monomer stability might be modulated by light in planta.

To further assess the localization and biological activity of wheat PHYC in planta, we transformed *Arabidopsis phyABCDE*-null mutant with *TmPHYC* fused to the red fluorescent protein DsRED (*TmPHYC*-DsRED). As a control, we transformed the same *Arabidopsis* mutant with a similar fusion between *Arabidopsis* PHYC and DsRED (*AtPHYC*-DsRED). Although undetectable in dark-grown seedlings, *TmPHYC*-DsRED could be detected as small fluorescent nuclear bodies after 4 h exposure to red light (Fig. 2C). Larger nuclear bodies were detected after longer light exposure and in seedlings grown in continuous light (Fig. 2C). Such nuclear bodies are similar to those observed in light-grown *Arabidopsis* plants transformed with *AtPHYB*-GFP (31). By contrast, no nuclear bodies are observed in the control plants transformed with the *Arabidopsis AtPHYC*-DsRED construct (SI Appendix, Fig. S6). This result is consistent with previous observations that *AtPHYC* is unstable in the absence of other phytochromes (23, 24).

Arabidopsis phyABCDE seedlings grown for 5 d under continuous red light are phenotypically similar to etiolated wild-type seedlings grown in the dark (Fig. 2D) (24). However, transformation of *Arabidopsis phyABCDE*-null mutant with *TmPHYC*-DsRED partially restored cotyledon opening and greening (Fig. 2D). Neither the presence of the wild-type *Arabidopsis PHYC* allele (24) nor overexpression of *AtPHYC*-DsRED could alter the etiolated phenotype of the *phyABCDE*-null mutant (Fig. 2D). Taken together, these results indicate that wheat PHYC can translocate into the *Arabidopsis* nucleus and mediate photomorphogenesis in the absence of other phytochromes.

Wheat *phyC^{AB}* Mutants Show Altered Expression Profiles of Photoperiod and Clock Genes. To establish the regulatory role of wheat *PHYC* in the photoperiodic flowering pathway, we examined the expression of key flowering regulators. Late flowering of wheat *phyC^{AB}* double mutant under LD correlates with a drastic reduction in transcript levels of the photoperiod genes *PPD1* and *FT1* (Fig. 3). Both genes are also slightly, but significantly, down-regulated in the *phyC^B* single mutant (SI Appendix, Fig. S2 B and C). In wild-type wheat, *PPD1* and *FT1* transcripts show diurnal cycles under LD and continuous light (LL), which disappear under continuous darkness (Fig. 3). In *phyC^{AB}* plants, by contrast, *PPD1* and *FT1* transcripts exhibit reduced transcript levels both in the presence and absence of light (Fig. 3) (LD and LL). These results indicate that light and PHYC are both required for transcriptional activation of *PPD1* and its downstream target *FT1*.

To test whether increased transcript levels of *FT1* compensate for the flowering delay associated with the *phyC^{AB}* mutants, the *phyC^{AB}* mutation and an *FT1* allele from the hexaploid wheat variety Hope (henceforth *FT1_{HOPE}*) were combined by three backcrosses into Kronos. The *FT1_{HOPE}* allele has a repetitive element in the promoter region that is associated with higher *FT1* transcript level than that of the wild-type allele, under both LD and SD photoperiods (32, 33). Indeed, wild-type and *phyC^{AB}* mutant plants carrying the *FT1_{HOPE}* allele show increased *FT1* transcript levels (SI Appendix, Fig. S7 A and B) and accelerated flowering relative to sibling lines carrying the *FT1* wild-type allele (SI Appendix, Fig. S7C). The differences in heading time between wild-type and *phyC^{AB}* mutant plants are reduced in the presence of the *FT1_{HOPE}* allele from 19 d to 1 d under SD and from 109 d to 100 d under LD (SI Appendix, Fig. S7C). Although the *FT1_{HOPE}* allele compensates poorly for the delayed flowering of the *phyC^{AB}* mutant, these results suggest that the difference in *FT1* expression contributes to the flowering phenotype of the *phyC^{AB}* mutants (Discussion).

PPD1, also known as *PRR37* in other grass species, is a member of the *PSEUDO RESPONSE REGULATOR* (*PRR*) gene family (25), which includes the clock genes *PRR73*, *PRR59*,

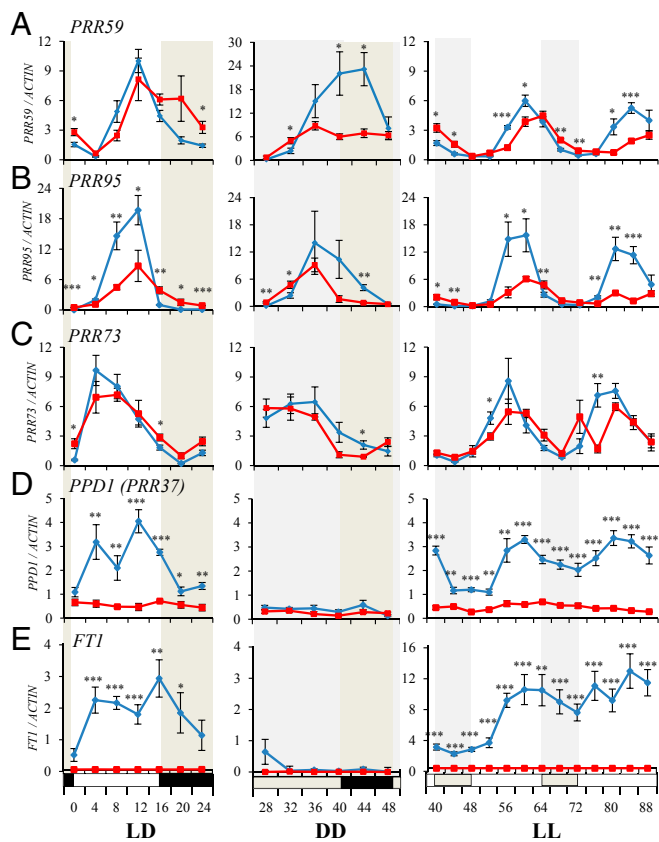


Fig. 3. Transcription profiles of *PRR* and photoperiod genes in wild type (blue lines) and *phyC^{AB}* mutant (red lines). (Left) Plants grown under long days (LD, 16 h light and 8 h dark, black rectangles). (Center) Plants transferred to continuous dark (DD). (Right) Plants transferred to continuous light (LL). DD and LL were at constant temperature. Gray rectangles indicate subjective nights in LL and subjective days in DD. (A) *PRR59*. (B) *PRR95*. (C) *PRR73*. (D) *PPD1* (= *PRR37*). (E) *FT1*. Error bars represent SEMs based on five plants. Asterisks indicate significant differences in *t* tests between wild type and *phyC^{AB}* at each time point (* $P < 0.05$, ** $P < 0.01$, and *** $P < 0.001$).

PRR95, and *TIMING OF CAB EXPRESSION* (*TOC1 = PRR1*). Although all of these *PRR* genes oscillate with a ~24-h period in the light, upon transfer to continuous darkness, circadian oscillations are observed for all *PRR* genes except *PPD1* (Fig. 3 and *SI Appendix, Fig. S8*). All of these *PRR* genes, as well as other important components of the circadian clock (e.g., *CIRCADIAN CLOCK ASSOCIATED1* (*CCA1*) and *GIGANTEA* (*GI*)) show significant differences in their oscillation profiles between wild-type and *phyC^{AB}* mutant plants (*SI Appendix, Fig. S8 A and C*) (34). Clock-output genes *CO1* and *CO2*, the wheat homologs of *Arabidopsis* photoperiod gene *CONSTANS* (*CO*), also exhibit altered transcriptional profiles in the *phyC^{AB}* mutant. Transcript levels of *CO1* are significantly higher in the *phyC^{AB}* mutant than in the wild type for most sampling points during long-day and continuous-light experiments (*SI Appendix, Fig. S8D*). By contrast, only a small phase shift of *CO2* transcript oscillation is observed in the *phyC^{AB}* mutant (*SI Appendix, Fig. S8E*).

Discussion

Wheat *PHYC* Encodes Dark-Stable Monomers and Signaling Active Homodimers in the Light. Rice and *Arabidopsis* *PHYC* proteins do not form stable homodimers and are degraded in the absence of *PHYB*-clade partners (13, 14, 23, 24). By contrast, wheat *PHYC* is able to form stable homodimers in yeast, in rice proplastids, and in transgenic *phyABCDE Arabidopsis* mutant plants

devoid of endogenous phytochromes. In the latter, we detected both *PHYC* monomers and homodimers in darkness (Fig. 2*B*) but mainly homodimers in the light, which implies that the balance between these two forms of *PHYC* may be dynamically modulated by light in planta.

The relative expression levels of *PHYC* and *PHYB* is an additional factor that may contribute to distinct signaling activity of *PHYC* in wheat and the two model plant species. Our studies show that the level of wheat *PHYC* expression is >10-fold higher than that of *PHYB* (*SI Appendix, Fig. S5*). In *Arabidopsis*, *PHYC* expression is considerably lower than that of *PHYB*: a result that has been corroborated at the protein level (35). By comparison, expression levels of *PHYB* and *PHYC* genes are more similar in rice (www.ncbi.nlm.nih.gov/geo; accession no. GSE36320). These expression differences are expected to alter the relative abundance of *PHYB* and *PHYC* proteins, thereby altering the accumulation of *PHYB:PHYC* heterodimers and *PHYB:PHYB* homodimers in the three plant species. Therefore, the effects of the loss of *PHYC* on *PHYB* signaling may be responsible in part for the different phenotypes of the *phyC* mutants in the three plant species. Additional studies are necessary to resolve the contributions of *PHYC* monomers, *PHYC* homodimers, *PHYB:PHYC* heterodimers, and/or *PHYB* homodimers to the flowering behavior of wheat.

We cannot rule out an unexpected function of mutant *PHYC* proteins to alter flowering time in wheat because the *PHYC^B* mutant protein does accumulate to wild-type levels (*SI Appendix, Fig. S1B*). We disfavor this hypothesis because the *phyC^B* mutant flowers only a few days later than the wild type whereas the *phyC^{AB}* double mutant exhibits a drastic delay to flower. Given that the *PHYC^A* truncated protein is undetectable in *phyC^{AB}* immunoblots (*SI Appendix, Fig. S1B*), the large delay in flowering of *phyC^{AB}* relative to *phyC^B* under LD is more consistent with the lack of a functional *PHYC* protein than with the gain-of-function activities of mutant *PHYC^B* proteins.

Variation in *PHYC* Correlates Well with Differences in Flowering Time.

The modest effect of the single *phyC^A* and *phyC^B* mutations on heading time contrasts with the large flowering delay observed in the *phyC^{AB}* double mutant and suggests that the two wheat *PHYC* homeologs have redundant functions. However, the stronger effect of *phyC^B* relative to *phyC^A* on flowering time indicates some degree of functional differentiation. Extensive sequence variation has been described in the A-genome copy of *PHYC^A* in hexaploid wheat, but very little is known about the natural variation in the other wheat *PHYC* homeologs (36). Given the stronger effect of *PHYC^B* on wheat flowering time, it is important to test whether its natural variation is associated with wheat adaptation to different latitudes or light environments. Indeed, allelic variation in *PHYC* is strongly associated with natural variation in flowering time for both *Arabidopsis* (37) and pearl millet (38). These results suggest that *PHYC* plays important roles in the adaptation of flowering plants to changing seasonal photoperiod.

Recently, a barley hyperfunctional *PHYC* allele has been linked to increased *FT1* abundance and accelerated flowering under inductive LD, but not under noninductive SD (16). Differences in heading time between plants carrying the hyperfunctional and wild-type *PHYC* alleles were suppressed by introgression of a highly expressed *FT1* allele (16). This result is similar to the reduced differences in heading time observed in this study between wheat wild type and *phyC^{AB}* mutants in the presence of the stronger *FT1_{HOPE}* allele (*SI Appendix, Fig. S7*). However, differences in *PPD1*, *GI*, and *CO1* transcript levels between the wild-type and *phyC^{AB}* mutant observed in our study (Fig. 3 and *SI Appendix, Fig. S8*) were not significant in the barley study (16). This difference is not surprising because wheat

phyC^{AB} mutants have no functional PHYC proteins whereas both barley alleles encode functional proteins.

The strong down-regulation of *FTI* in the wheat *phyC^{AB}* mutants is in good agreement with the undetectable level of *FTI* reported for *T. monococcum mvp* mutants, which have a large deletion encompassing both *PHYC* and *VRN1* genes (15, 18). The *mvp* mutants also have a complete deletion of *VRN2*, which led Shimada et al. (22) to hypothesize that the down-regulation of *FTI* in this mutant was caused by the deletion of *VRN1*. However, a subsequent study in tetraploid wheat showed that plants carrying nonfunctional copies of *VRN1* and *VRN2* (but normal *PHYC* alleles) flower as early as some spring wheats (65 d after sowing) and have high levels of *FTI* expression (21). By contrast, we show that loss-of-function mutations in *PHYC* are sufficient to down-regulate *FTI* to almost undetectable levels (Fig. 3E). Taken together, these results suggest that the down-regulation of *FTI* in the *mvp* mutants is more likely caused by the deletion of *PHYC* than by the deletion of *VRN1*. However, the nonflowering phenotype of the *mvp* mutant cannot be explained solely by the deletion of *PHYC* because the *phyC^{AB}* mutant in Kronos eventually flowers. The nonflowering phenotype of the *mvp* mutant may be caused by the simultaneous deletion of *PHYC* and *VRN1* or, alternatively, by the deletion of additional genes located inside the large deletion present in the *mvp* mutant (e.g., the MADS-box gene *AGLGI*) (18).

PHYC Is Involved in the Transcriptional Regulation of both Photoperiod and Clock Genes. Most of the natural variation in photoperiod sensitivity in wheat and barley is associated with mutations in *PPD1*, which is considered to be the central photoperiod gene in both species (25, 39–41). Hexaploid wheat plants carrying nonfunctional alleles of all three *PPD1* homeologs flower almost 1 mo later than their wild-type sibling lines, a result that confirms the critical role of *PPD1* in the acceleration of wheat flowering under LD (42). Therefore, the significant down-regulation of *PPD1* in the *phyC^{AB}* plants (Fig. 3 and *SI Appendix, Fig. S7D*) is likely to contribute to their late flowering phenotype. Our expression data show that wheat *PPD1* transcription requires light because its transcript levels and circadian oscillations are both strongly attenuated in continuous darkness (Fig. 3). *PPD1* expression also requires PHYC because *PPD1* transcript levels in *phyC^{AB}* mutant plants grown under LD or LL are reduced to levels similar to those observed in wild-type plants grown in continuous darkness (Fig. 3). Taken together, these results suggest that the transcriptional activation of *PPD1* by light is mediated by *PHYC*.

Down-regulation of *PPD1* is the most likely cause of the drastic reduction of *FTI* transcript levels in the *phyC^{AB}* plants (Fig. 3) because a similar down-regulation of *FTI* is observed in the *ppd1*-null hexaploid wheat plants (42). Mutations in both *FTI* homologs in Kronos also delay flowering by 25 d under LD (43); thus, down-regulation of *FTI* in the *phyC^{AB}* Kronos mutant contributes to its late flowering. This hypothesis is supported by the smaller difference in heading time between *phyC^{AB}* mutant and wild-type alleles in the presence of the *FTI_{HOPE}* allele than in the presence of the *FT* wild-type alleles. However, even in the presence of the stronger *FTI_{HOPE}* allele, *FTI* transcript levels in the *phyC^{AB}* mutant are still 100-fold lower than those in the wild type, accounting for their late flowering time (*SI Appendix, Fig. S7*). This last result suggests that the insertion of the repetitive element in the promoter of the *FTI_{HOPE}* allele is unable to fully compensate for the low expression of *PPD1* in the *phyC^{AB}* mutant.

The delay in heading time observed in the tetraploid *phyC^{AB}* mutant under LD is more than threefold longer than that observed in the triple *ppd1*-null mutant in hexaploid wheat (42) and that reported for the *FTI* mutants in tetraploid Kronos (43). This result suggests that additional genes regulated by PHYC

contribute to early flowering of wheat under LD. Indeed, our expression data show that the *phyC^{AB}* mutant has altered expression profiles of circadian clock genes (Fig. 3 and *SI Appendix, Fig. S8*), which are known to regulate a large number of plant genes (44). Thus, misexpression of multiple clock-output genes may also contribute to the delayed flowering of the *phyC^{AB}* mutant under LD. Transcriptional changes of the clock genes observed in the *phyC^{AB}* mutant are independent of the down-regulation of *PPD1* because no consistent changes in the transcription profiles of the same clock genes have been observed in *ppd1* mutants of barley or wheat (45, 46).

Among circadian clock output genes, *CO1* and *CO2* are of particular interest due to the central role of the *Arabidopsis* (*CO*) and rice homolog (*HDI*) on photoperiodic regulation of flowering time (47, 48). Direct comparison of *CO1* and *CO2* with CO-related proteins in other species is complicated by duplication of these genes in the *Triticeae* lineage (49) and by limited functional information. However, we observed that *CO1* and *CO2* transcription profiles are altered in the *phyC^{AB}* mutant relative to the wild type (*SI Appendix, Fig. S8*). Because neither *CO1* nor *CO2* is fully down-regulated in continuous darkness (*SI Appendix, Fig. S9*), PHYC-regulation of both genes appears to be independent of its regulation of *PPD1* (Fig. 4).

Previous studies suggest that *CO1* and *CO2* play some role in the regulation of flowering time in the temperate cereals. Transgenic expression of a genomic copy of wheat *CO2* in a rice *hd1* (= *co*) mutant restores *HDI* function, accelerating heading time under SD and delaying it under LD (50). This complementation study indicates that wheat *CO2* encodes a functional protein that shares common structure and function with rice *HD1* (50). Overexpression of barley *CO1* in barley results in accelerated flowering time under LD (51), suggesting that *CO1* promotes flowering. However, CO overexpression results should be interpreted with caution because overexpression of *HDI* in rice results in delayed flowering time under SD even though this gene naturally works as a flowering promoter under SD (52). These conflicting results suggest that a precise spatial and/or temporal expression of CO homologs and/or a precise balance of their relative protein levels with other partners are required for their characteristic functions in different species.

PHYC Plays Distinct Roles in the Regulation of Flowering Time in Different Plant Species. The external coincidence model postulates that the convergence of external light signals and internal clock oscillations is required to measure day length (53). In *Arabidopsis*, the induction of *FT* by CO occurs only under LD, when a transcriptional peak in CO circadian rhythm coincides with the external exposure to light, which is required to stabilize the CO protein (54, 55). In rice, expression of *HDI* (= *CO*) is also under the control of the circadian clock (56). Changes in the external coincidence of the circadian peaks of *HDI* expression with light-activated Pfr forms of PHYB or PHYC contribute to the seasonal photoperiod responses in rice (52, 56). The essential role of phytochromes in the perception of day length in rice is well established by the complete loss of photoperiodic response in the *photoperiodic sensitivity 5* (*se5*) mutant that lacks all photo-reversible phytochromes (57).

We show here that circadian clock and external light signals also converge to regulate transcript abundance of the wheat photoperiod gene *PPD1* (Fig. 3). A similar convergence has been described in the regulation of the sorghum *PPD1* homolog *PRR37* (= *Ma₁*), a gene that has a large impact on sorghum flowering time and has been critical for the early domestication and dispersal of this species (58). Mutations in *PPD1/PRR37* are associated with photoperiod insensitivity genotypes both in sorghum and wheat, suggesting that this gene is critical for the perception of day-length differences in different grass species. In rice, natural variation in *PRR37* also contributes to differences in

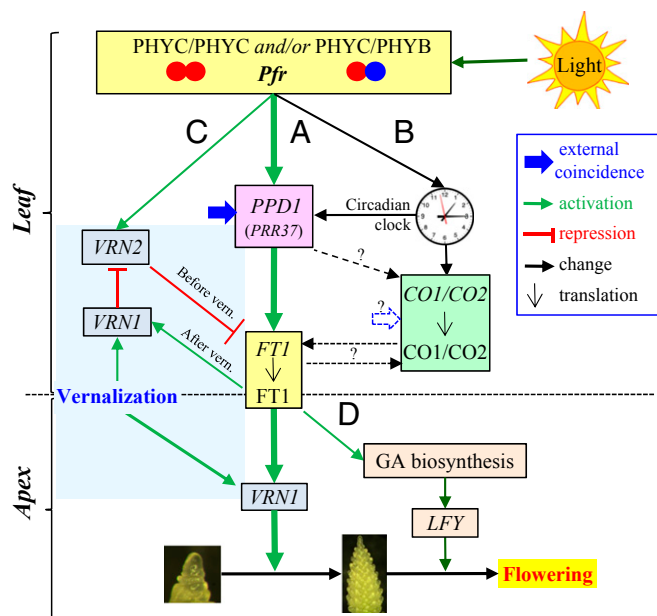


Fig. 4. An integrated model of wheat flowering regulation under LD. Three pathways regulate the expression of *FT* under LD in rice (59) and sorghum (58, 70), and a similar model is proposed here for wheat. We propose that light-activated Pfr forms of PHYC (homo- or heterodimers) operate upstream of these three different pathways, identified with the letters A to D. (Pathway A) The central pathway, indicated by thicker arrows, has the largest effect on the acceleration of flowering under LD. The PHYC-mediated light activation of *PPD1* results in the convergence of light and circadian clock signals in the transcriptional regulation of *PPD1*, which is critical for measurement of day length, according to the external coincidence model (blue arrow). Under LD, *PPD1/PRR37* up-regulates *FT1* in barley and wheat (25) but down-regulates *FT* homologs in rice and sorghum (58, 59). Up-regulation of *FT1* in wheat is associated with the up-regulation of *FT2* (43, 71), which also promotes flowering (72). (Pathway B) PHYC also modulates the expression of circadian clock and clock output genes *CO1* and *CO2*. The role of these genes on wheat flowering is still not well understood, but the *Arabidopsis* (*CO*) and rice (*HD1*) homologs are involved in the photoperiodic regulation of *FT* (47, 48). Tentatively, a similar role is hypothesized in wheat (dotted blue arrow). (Pathways A and B) *PPD1* mutations in wheat affect *CO1* transcription suggesting a crosstalk between the A and B pathways (either directly or indirectly through a feedback effect of *FT1*, dotted black lines) (42, 45). (Pathway C) *VRN2* is a long-day repressor of *FT1* that prevents flowering in the fall (73, 74). *VRN2* is transcribed only in the light (18) and is down-regulated in the presence of the *phyC^B* mutation ($P < 0.0001$) (*SI Appendix, Fig. S11*), which suggests that the light activation of *VRN2* transcription is mediated by PHYC. This hypothesis is further supported by the drastic down-regulation of *VRN2* transcription in the *mvp* mutants with a deleted PHYC gene (18). *VRN2* and *PPD1* compete for the activation of *FT1*, but the repressing effect of *VRN2* is epistatic to the promoting effect of *PPD1*, preventing flowering in the fall. Long exposures to cold temperatures during the winter (vernalization) result in the up-regulation of *VRN1* in both apices and leaves (19, 75). In the apex, *VRN1* initiates the transition of the shoot apical meristem to the reproductive stage whereas, in the leaves, it acts as a transcriptional repressor of *VRN2* (21). The down-regulation of *VRN2* results in the up-regulation of *FT1* by *PPD1* and the acceleration of flowering during the longer days of spring. The up-regulation of *FT1* in the leaves further induces *VRN1* (71), closing a positive feedback loop that accelerates flowering under LD (21, 76). (Pathway D) In the apex, *FT1* induces *VRN1* transcription and gibberellin biosynthesis and accumulation (33). The simultaneous presence of gibberellin and *VRN1* results in the up-regulation of *SOC1-1* and *LFY*, which are required for normal wheat-spike development. The regulation of gibberellin biosynthesis in the apex by *FT1* acts as a secondary LD regulatory point (33).

photoperiodic response and to its ability to grow in a wide range of latitudes (59). The duplication that originated *PRR37* and *PRR73* in the grasses is independent of the duplication that generated *PRR3* and *PRR7* genes in *Arabidopsis* (60). Thus,

subfunctionalization of *PRR37* into a photoperiod gene probably occurred in the grass lineage after their separation from the eudicots, which may explain why this second photoperiod pathway has not been detected in *Arabidopsis* (60).

Plants that flower earlier when day length exceeds a critical photoperiod are classified as LD plants (e.g., *Arabidopsis* and wheat) whereas those that flower earlier when day lengths are less than a critical photoperiod are classified as SD plants (e.g., rice and sorghum). Differences between these two classes are mainly determined by signal reversals of the photoperiod genes on the regulation of *FT/HD3A*. Under LD, *CO/HD1* acts as a suppressor of *HD3A* and flowering in rice (56, 61, 62). Similarly, *PPD1/PRR37* induces *FT1* and accelerates flowering in barley and wheat (25, 42) but suppresses *FT* and delays flowering in sorghum and rice (58, 59). This signal reversal in *PPD1/PRR37* may explain why *phyC* mutations accelerate flowering under LD in rice (13) but delay flowering in wheat (Fig. 1). The role of PHYC also differs between wheat and *Arabidopsis* under non-inductive SD photoperiod. Under this condition, a nonfunctional PHYC mutation accelerates flowering in *Arabidopsis* by 22.5 d (14) but delays flowering in Kronos by 18 d (Fig. 1D). Because the *Ppd-A1a* allele present in Kronos is misexpressed under SD (41), it would be interesting to test whether this difference is maintained in a Kronos isogenic line carrying the wild-type *Ppd-A1b* allele. Taken together, these comparative analyses underscore the plasticity of plant flowering pathways, which have evolved to optimize reproduction under a wide range of photoperiods and temperatures.

A Model for the PHYC-Mediated Regulation of Flowering in Wheat and Future Directions. To integrate the results from this study into the current knowledge of the regulation of wheat flowering time under LD, we propose a hypothetical model that is described in detail in Fig. 4. This model highlights the central role of PHYC in the light activation of *PPD1* and *FT1* under LD. It also describes additional roles of PHYC on the regulation of the circadian clock (Fig. 3 and *SI Appendix, Fig. S8*) and on the light activation of the vernalization gene *VRN2*, a homolog of rice LD-flowering repressor *Ghd7* (63) (*SI Appendix, Fig. S11*).

This model also identifies areas that require additional research. The relative contribution of wheat PHYC and PHYB homo- and heterodimers to the observed differences in flowering remains an important unanswered question. The possible effects of PHYC on the stability of proteins encoded by photoperiod and circadian clock genes and on the specific roles of clock output genes *CO1* and *CO2* in the regulation of wheat flowering remain important questions for future studies.

The central question that remains unanswered is how PHYC contributes to the perception of day length. Because Pfr slowly reverts to the Pr form in the absence of light ("dark reversion"), it has been argued to function as a sand timer to measure the length of the night period (64). Dark reversion also provides the means for light and temperature signals to be integrated. It is also possible that the perception of day length via the external coincidence mechanism is controlled by a gene regulated by PHYC (e.g., *PPD1*). Despite the pending questions, the discovery of the central role of PHYC in the regulation of the photoperiod response in wheat improves our understanding of reproductive development in this economically important species. A detailed characterization of the gene networks that regulate wheat flowering will accelerate the development of wheat varieties better adapted to new and changing environments.

Materials and Methods

Materials. The tetraploid wheat variety Kronos used in this study has a spring growth habit determined by the *Vrn-A1c* allele. This allele has a large deletion in the first intron (65), which greatly reduces the vernalization

requirement (65). In addition, Kronos carries the dominant *Ppd-A1a* allele, which has a 1,027-bp deletion in the promoter region that is not present in the wild-type *Ppd-A1b* allele. Previous studies have shown that, under SD, the presence of the *Ppd-A1a* allele is associated with significantly higher levels of *PPD1* expression in the dark and early morning, and with 30–40 d acceleration of flowering relative to the *Ppd-A1b* allele (41). The *Ppd-A1a* allele is referred to in the wheat literature as “photoperiod-insensitive” because the accelerated flowering under SD reduces the differences between LD and SD relative to the “photoperiod-sensitive” *Ppd-A1b* allele. However, Kronos plants carrying the *Ppd-A1a* allele flower more than 40 d earlier when grown under LD than when grown under SD, demonstrating that plants carrying the *Ppd-A1a* allele are still photoperiod-sensitive. Under LD, the differences in heading time between the *Ppd-A1a* and *Ppd-A1b* alleles are very small, both in a wild-type Kronos and in a *phyC^{AB}* mutant background (*SI Appendix, Fig. S10*).

Mutant Screen. A TILLING (for Targeting Local Lesions IN Genomes) population of 1,368 lines of the tetraploid wheat cultivar “Kronos” mutagenized with ethyl methane sulphonate (EMS) (28) was screened for mutations in the A and B genome copies of *PHYC* using genome-specific primers described in *SI Appendix, Table S1*. We selected *PHYC^A* mutant T4-2327 and *PHYC^B* mutant T4-807 (*SI Appendix, Table S3 and Fig. S1*), backcrossed them for two generations to Kronos to reduce background mutations, and combined the two loss-of-function mutations in the *phyC^{AB}* double mutant. The morphological characterization of the mutants is described in *SI Appendix, SI Materials and Methods and Table S6*.

qRT-PCR. RNA samples were extracted from leaves using the Spectrum Plant Total RNA Kit (Sigma-Aldrich). Quantitative PCR was performed using SYBR Green and a 7500 Fast Real-Time PCR system (Applied Biosystems). *ACTIN* was used as an endogenous control. Primers and their efficiency are listed in *SI Appendix, Table S5*. qRT-PCR primers were designed in exon junctions to avoid genomic DNA amplification. Transcript levels for all genes and experiments presented in this study are expressed as linearized fold-*ACTIN* levels calculated by the formula $2^{(ACTIN_{CT} - TARGET_{CT})} \pm SE$ of the mean. The resulting number indicates the ratio between the initial number of molecules of the target gene and the number of molecules of *ACTIN*. Therefore, the Y scales are comparable across genes and experiments.

Yeast Two-Hybrid Assays. Yeast vectors pGBKT7 and pGADT7 (Clontech) were used for all constructs. Yeast strain Y2H Gold was used in the yeast two-hybrid (Y2H) assays. Full-length *PHYC* from *T. monococcum* (*TmPHYC*), the N-terminal coding region (N-*TmPHYC*, amino acids 1–600 including the PAS, GAF, and PHY domains), and the C-terminal coding region (C-*TmPHYC*, amino acids 601–1139, including two PAS and the histidine kinase-like ATPase domains) were cloned into pGBKT7 and pGADT7 vectors between restriction sites NdeI and XmaI, using primers listed in *SI Appendix, Table S8*. The C-terminal coding region of the *Arabidopsis* *PHYC* (C-*AtPHYC*, amino acids 601–1111, GenBank accession no. AED94021.1) was cloned from the Columbia ecotype and inserted into pGBKT7 and pGADT7 linearized with NdeI and XmaI restriction enzymes. The full-length *TmPHYB* coding region from

T. monococcum was cloned into pGADT7 between restriction sites EcoRI and SpeI. All constructs were verified by DNA sequencing.

Transformation of an *Arabidopsis* *phy*-Null Mutant with Wheat *PHYC*. To study wheat *PHYC* protein in the absence of other phytochromes, we generated a *TmPHYC*-FLAG fusion by adding a 3xFLAG tag (Sigma-Aldrich) to the C terminus of the complete coding region of *PHYC* from diploid wheat *T. monococcum* accession DV92. The sequence encoding the *TmPHYC*-FLAG fusion was then inserted downstream of the CaMV35S promoter between restriction sites XbaI and SacI of the binary vector pGWB14 (66) (primers used in construct generation are listed in *SI Appendix, Table S9*). We transformed this 35S::*TmPHYC*-FLAG construct into an *Arabidopsis* *phy*-null mutant with no active phytochromes (*phyABCDE*) (24) using the floral dip method (67).

To study the subcellular localization of wheat *PHYC* in planta, we fused the fluorescent protein DsRED (68) to the C terminus of the full-length wheat *TmPHYC* protein (primers used to generate the constructs are listed in *SI Appendix, Table S9*) and transformed it into the *Arabidopsis* *phyABCDE* mutant (24). *Arabidopsis* transgenic plants transformed with the 35S::*TmPHYC*-DsRED construct were analyzed using an Olympus FV1000 confocal laser-scanning microscope. Excitation and emission wavelengths were 543 nm and 580 nm, respectively. To study the dynamics of the light-induced nuclear import and nuclear body formation of the wheat *PHYC*, we grew the transgenic *Arabidopsis* plants in the dark for 5 d and then exposed the etiolated plants to 50 $\mu\text{mol}\cdot\text{m}^{-2}\cdot\text{s}^{-1}$ red light (R) and collected images at 0 h, 4 h, 6 h, and 21 h. Transgenic plants grown under continuous red light for 5 d served as positive control. For the comparison of *TmPHYC*-DsRED and *Arabidopsis* *AtPHYC*-DsRED in *phyABCDE*, positively transformed *Arabidopsis* mutants were transferred to continuous white light ($Wc \approx 60 \mu\text{mol}\cdot\text{m}^{-2}\cdot\text{s}^{-1}$) for 1 d before images were taken (*SI Appendix, Fig. S6*).

Native Electrophoresis, Immunoblots, and Antibodies. Total protein was extracted from fresh dark- or light-grown 10-d-old *Arabidopsis* seedlings as described before (69). Proteins samples were separated on 4–15% gradient TGX gels (Bio-Rad) in native PAGE buffer (25 mM Tris, 192 mM glycine) for 40 h at 4 °C, blotted to polyvinylidene difluoride (PVDF) membrane, and hybridized with Anti-FLAG antibody (Sigma) at a dilution of 1:1,000. A second antibody against rice *PHYC* (Anti-OsPhyC) (13) was also used for native Western blot analysis at a dilution of 1:1,500. Chemiluminescent detection of primary antibodies was performed with horseradish peroxidase-conjugated secondary antibody and ECL detection reagents (GE Healthcare) and captured by ChemiDoc-It imager (UVP).

ACKNOWLEDGMENTS. We thank Dr. Makoto Takano (National Institute of Agrobiological Sciences, Tsukuba, Japan) for the rice *PHYC* antibody and Dr. Naohiro Kato (Louisiana State University) for split luciferase vectors. This project was supported by the Howard Hughes Medical Institute, the Gordon and Betty Moore Foundation, National Research Initiative Grants 2011-67013-30077 and 2011-68002-30029 from the US Department of Agriculture National Institute of Food and Agriculture (to J.D.), and National Institutes of Health Grant R01 GM068552 (to J.C.L.).

- Rockwell NC, Su YS, Lagarias JC (2006) Phytochrome structure and signaling mechanisms. *Annu Rev Plant Biol* 57:837–858.
- Chen M, Chory J (2011) Phytochrome signaling mechanisms and the control of plant development. *Trends Cell Biol* 21(11):664–671.
- Jiao Y, Lau OS, Deng XW (2007) Light-regulated transcriptional networks in higher plants. *Nat Rev Genet* 8(3):217–230.
- Quail PH (2007) Phytochrome-regulated gene expression. *J Integr Plant Biol* 49:11–20.
- Nagatani A (2004) Light-regulated nuclear localization of phytochromes. *Curr Opin Plant Biol* 7(6):708–711.
- Hughes J (2013) Phytochrome cytoplasmic signaling. *Annu Rev Plant Biol* 64:377–402.
- Mathews S (2010) Evolutionary studies illuminate the structural-functional model of plant phytochromes. *Plant Cell* 22(1):4–16.
- Sharrack RA (2008) The phytochrome red/far-red photoreceptor superfamily. *Genome Biol* 9(8):230.
- Casal JJ, Candia AN, Sellaro R (2013) Light perception and signalling by phytochrome A. *J Exp Bot* 10.1093/jxb/ert379.
- Franklin KA, Quail PH (2010) Phytochrome functions in Arabidopsis development. *J Exp Bot* 61(1):11–24.
- Casal JJ (2013) Photoreceptor signaling networks in plant responses to shade. *Annu Rev Plant Biol* 64:403–427.
- Franklin KA, Davis SJ, Stoddart WM, Vierstra RD, Whitelam GC (2003) Mutant analyses define multiple roles for phytochrome C in Arabidopsis photomorphogenesis. *Plant Cell* 15(9):1981–1989.
- Takano M, et al. (2005) Distinct and cooperative functions of phytochromes A, B, and C in the control of deetiolation and flowering in rice. *Plant Cell* 17(12):3311–3325.
- Monte E, et al. (2003) Isolation and characterization of *phyC* mutants in Arabidopsis reveals complex crosstalk between phytochrome signaling pathways. *Plant Cell* 15(9):1962–1980.
- Shitsukawa N, et al. (2007) The einkorn wheat (*Triticum monococcum*) mutant, *maintained vegetative phase*, is caused by a deletion in the *VRN1* gene. *Genes Genet Syst* 82(2):167–170.
- Nishida H, et al. (2013) Phytochrome C is a key factor controlling long-day flowering in barley. *Plant Physiol* 163(2):804–814.
- Szucs P, et al. (2006) Positional relationships between photoperiod response QTL and photoreceptor and vernalization genes in barley. *Theor Appl Genet* 112(7):1277–1285.
- Distelfeld A, Dubcovsky J (2010) Characterization of the *maintained vegetative phase* deletions from diploid wheat and their effect on *VRN2* and *FT* transcript levels. *Mol Genet Genomics* 283(3):223–232.
- Yan L, et al. (2003) Positional cloning of the wheat vernalization gene *VRN1*. *Proc Natl Acad Sci USA* 100(10):6263–6268.
- Trevaskis B, Bagnall DJ, Ellis MH, Peacock WJ, Dennis ES (2003) MADS box genes control vernalization-induced flowering in cereals. *Proc Natl Acad Sci USA* 100(22):13099–13104.
- Chen A, Dubcovsky J (2012) Wheat TILLING mutants show that the vernalization gene *VRN1* down-regulates the flowering repressor *VRN2* in leaves but is not essential for flowering. *PLoS Genet* 8(12):e1003134.
- Shimada S, et al. (2009) A genetic network of flowering-time genes in wheat leaves, in which an *APETALA1/FRUITFULL*-like gene, *VRN1*, is upstream of *FLOWERING LOCUS T*. *Plant J* 58(4):668–681.

23. Clack T, et al. (2009) Obligate heterodimerization of Arabidopsis phytochromes C and E and interaction with the PIF3 basic helix-loop-helix transcription factor. *Plant Cell* 21(3):786–799.
24. Hu W, et al. (2013) Unanticipated regulatory roles for Arabidopsis phytochromes revealed by null mutant analysis. *Proc Natl Acad Sci USA* 110(4):1542–1547.
25. Turner A, Beales J, Faure S, Dunford RP, Laurie DA (2005) The pseudo-response regulator *Ppd-H1* provides adaptation to photoperiod in barley. *Science* 310(5750):1031–1034.
26. Corbesier L, et al. (2007) FT protein movement contributes to long-distance signaling in floral induction of Arabidopsis. *Science* 316(5827):1030–1033.
27. Tamaki S, Matsuo S, Wong HL, Yokoi S, Shimamoto K (2007) Hd3a protein is a mobile flowering signal in rice. *Science* 316(5827):1033–1036.
28. Uauy C, et al. (2009) A modified TILLING approach to detect induced mutations in tetraploid and hexaploid wheat. *BMC Plant Biol* 9:115–128.
29. Matsushita T, Mochizuki N, Nagatani A (2003) Dimers of the N-terminal domain of phytochrome B are functional in the nucleus. *Nature* 424(6948):571–574.
30. Rockwell NC, Martin SS, Feoktistova K, Lagarias JC (2011) Diverse two-cysteine photocycles in phytochromes and cyanobacteriochromes. *Proc Natl Acad Sci USA* 108(29):11854–11859.
31. Yamaguchi R, Nakamura M, Mochizuki N, Kay SA, Nagatani A (1999) Light-dependent translocation of a phytochrome B-GFP fusion protein to the nucleus in transgenic Arabidopsis. *J Cell Biol* 145(3):437–445.
32. Yan L, et al. (2006) The wheat and barley vernalization gene *VRN3* is an orthologue of *FT*. *Proc Natl Acad Sci USA* 103(51):19581–19586.
33. Pearce S, Vanzetti LS, Dubcovsky J (2013) Exogenous gibberellins induce wheat spike development under short days only in the presence of *VERNALIZATION1*. *Plant Physiol* 163(3):1433–1445.
34. Nagel DH, Kay SA (2012) Complexity in the wiring and regulation of plant circadian networks. *Curr Biol* 22(16):R648–R657.
35. Sharrock RA, Clack T (2002) Patterns of expression and normalized levels of the five Arabidopsis phytochromes. *Plant Physiol* 130(1):442–456.
36. Beales J, Laurie DA, Devos KM (2005) Allelic variation at the linked *AP1* and *PhyC* loci in hexaploid wheat is associated but not perfectly correlated with vernalization response. *Theor Appl Genet* 110(6):1099–1107.
37. Balasubramanian S, et al. (2006) The PHYTOCHROME C photoreceptor gene mediates natural variation in flowering and growth responses of *Arabidopsis thaliana*. *Nat Genet* 38(6):711–715.
38. Saidou A-A, et al. (2014) Association mapping, patterns of linkage disequilibrium and selection in the vicinity of the PHYTOCHROME C gene in pearl millet. *Theor Appl Genet* 127(1):19–32.
39. Beales J, Turner A, Griffiths S, Snape JW, Laurie DA (2007) A pseudo-response regulator is misexpressed in the photoperiod insensitive *Ppd-D1a* mutant of wheat (*Triticum aestivum* L.). *Theor Appl Genet* 115(5):721–733.
40. Diaz A, Zikhali M, Turner AS, Isaac P, Laurie DA (2012) Copy number variation affecting the *Photoperiod-B1* and *Vernalization-A1* genes is associated with altered flowering time in wheat (*Triticum aestivum*). *PLoS ONE* 7(3):e33234.
41. Wilhelm EP, Turner AS, Laurie DA (2009) Photoperiod insensitive *Ppd-A1a* mutations in tetraploid wheat (*Triticum durum* Desf.). *Theor Appl Genet* 118(2):285–294.
42. Shaw LM, Turner AS, Herry L, Griffiths S, Laurie DA (2013) Mutant alleles of *Photoperiod-1* in wheat (*Triticum aestivum* L.) that confer a late flowering phenotype in long days. *PLoS ONE* 8(11):e79459.
43. Lv B, et al. (2014) Characterization of *FLOWERING LOCUS T1 (FT1)* gene in *Brachypodium* and wheat. *PLoS ONE* 9(4):e94171.
44. Schaffer R, et al. (2001) Microarray analysis of diurnal and circadian-regulated genes in Arabidopsis. *Plant Cell* 13(1):113–123.
45. Shaw LM, Turner AS, Laurie DA (2012) The impact of photoperiod insensitive *Ppd-1a* mutations on the photoperiod pathway across the three genomes of hexaploid wheat (*Triticum aestivum*). *Plant J* 71(1):71–84.
46. Campoli C, Shtaya M, Davis SJ, von Korff M (2012) Expression conservation within the circadian clock of a monocot: natural variation at barley *Ppd-H1* affects circadian expression of flowering time genes, but not clock orthologs. *BMC Plant Biol* 12:97.
47. Putterill J, Robson F, Lee K, Simon R, Coupland G (1995) The *CONSTANS* gene of *Arabidopsis* promotes flowering and encodes a protein showing similarities to zinc finger transcription factors. *Cell* 80(6):847–857.
48. Takahashi Y, Teshima KM, Yokoi S, Innan H, Shimamoto K (2009) Variations in Hd1 proteins, Hd3a promoters, and *Ehd1* expression levels contribute to diversity of flowering time in cultivated rice. *Proc Natl Acad Sci USA* 106(11):4555–4560.
49. Griffiths S, Dunford RP, Coupland G, Laurie DA (2003) The evolution of *CONSTANS*-like gene families in barley, rice, and Arabidopsis. *Plant Physiol* 131(4):1855–1867.
50. Nemoto Y, Kisaka M, Fuse T, Yano M, Ogihara Y (2003) Characterization and functional analysis of three wheat genes with homology to the *CONSTANS* flowering time gene in transgenic rice. *Plant J* 36(1):82–93.
51. Campoli C, Drosse B, Searle I, Coupland G, von Korff M (2012) Functional characterisation of *HvCO1*, the barley (*Hordeum vulgare*) flowering time ortholog of *CONSTANS*. *Plant J* 69(5):868–880.
52. Ishikawa R, et al. (2011) Phytochrome B regulates *Heading date 1 (Hd1)*-mediated expression of rice florigen *Hd3a* and critical day length in rice. *Mol Genet Genomics* 285(6):461–470.
53. Pittendrigh CS, Minis DH (1964) The entrainment of circadian oscillations by light and their role as photoperiodic clocks. *Am Nat* 98:261–294.
54. Turck F, Fornara F, Coupland G (2008) Regulation and identity of florigen: FLOWERING LOCUS T moves center stage. *Annu Rev Plant Biol* 59:573–594.
55. Valverde F, et al. (2004) Photoreceptor regulation of *CONSTANS* protein in photoperiodic flowering. *Science* 303(5660):1003–1006.
56. Izawa T, et al. (2002) Phytochrome mediates the external light signal to repress FT orthologs in photoperiodic flowering of rice. *Genes Dev* 16(15):2006–2020.
57. Izawa T, Oikawa T, Tokutomi S, Okuno K, Shimamoto K (2000) Phytochromes confer the photoperiodic control of flowering in rice (a short-day plant). *Plant J* 22(5):391–399.
58. Murphy RL, et al. (2011) Coincident light and clock regulation of pseudoreponse regulator protein 37 (PRR37) controls photoperiodic flowering in sorghum. *Proc Natl Acad Sci USA* 108(39):16469–16474.
59. Koo BH, et al. (2013) Natural variation in OsPRR37 regulates heading date and contributes to rice cultivation at a wide range of latitudes. *Mol Plant* 6(6):1877–1888.
60. Farré EM, Liu T (2013) The PRR family of transcriptional regulators reflects the complexity and evolution of plant circadian clocks. *Curr Opin Plant Biol* 16(5):621–629.
61. Hayama R, Yokoi S, Tamaki S, Yano M, Shimamoto K (2003) Adaptation of photoperiodic control pathways produces short-day flowering in rice. *Nature* 422(6933):719–722.
62. Ishikawa R, et al. (2005) Suppression of the floral activator *Hd3a* is the principal cause of the night break effect in rice. *Plant Cell* 17(12):3326–3336.
63. Xue W, et al. (2008) Natural variation in *Ghd7* is an important regulator of heading date and yield potential in rice. *Nat Genet* 40(6):761–767.
64. Vince-Prue D (1994) *The Duration of Light and Photoperiodic Responses: Photomorphogenesis in Plants* (Martinus Nijhoff, Dordrecht, The Netherlands), 2nd Ed, pp 447–490.
65. Fu D, et al. (2005) Large deletions within the first intron in *VRN-1* are associated with spring growth habit in barley and wheat. *Mol Genet Genomics* 273(1):54–65.
66. Nakagawa T, et al. (2007) Development of series of gateway binary vectors, pGWBs, for realizing efficient construction of fusion genes for plant transformation. *J Biosci Bioeng* 104(1):34–41.
67. Clough SJ, Bent AF (1998) Floral dip: A simplified method for *Agrobacterium*-mediated transformation of *Arabidopsis thaliana*. *Plant J* 16(6):735–743.
68. Smit P, et al. (2005) NSP1 of the GRAS protein family is essential for rhizobial Nod factor-induced transcription. *Science* 308(5729):1789–1791.
69. Sharrock RA, Clack T (2004) Heterodimerization of type II phytochromes in Arabidopsis. *Proc Natl Acad Sci USA* 101(31):11500–11505.
70. Murphy RL, et al. (2014) *Ghd7* (Ma6) represses sorghum flowering in long days: *Ghd7* alleles enhance biomass accumulation and grain production. *Plant Gen*, 10.3835/plantgenome2013.11.0040.
71. Li C, Dubcovsky J (2008) Wheat FT protein regulates *VRN1* transcription through interactions with FDL2. *Plant J* 55(4):543–554.
72. Wu L, et al. (2013) Regulation of *FLOWERING LOCUS T* by a microRNA in *Brachypodium distachyon*. *Plant Cell* 25(11):4363–4377.
73. Dubcovsky J, et al. (2006) Effect of photoperiod on the regulation of wheat vernalization genes *VRN1* and *VRN2*. *Plant Mol Biol* 60(4):469–480.
74. Trevaskis B, Hemming MN, Peacock WJ, Dennis ES (2006) *HvVRN2* responds to day-length, whereas *HvVRN1* is regulated by vernalization and developmental status. *Plant Physiol* 140(4):1397–1405.
75. Oliver SN, Finnegan EJ, Dennis ES, Peacock WJ, Trevaskis B (2009) Vernalization-induced flowering in cereals is associated with changes in histone methylation at the *VERNALIZATION1* gene. *Proc Natl Acad Sci USA* 106(20):8386–8391.
76. Loukoianov A, Yan L, Blechl A, Sanchez A, Dubcovsky J (2005) Regulation of *VRN-1* vernalization genes in normal and transgenic polyploid wheat. *Plant Physiol* 138(4):2364–2373.

Supplementary Materials for
**PHYTOCHROME C plays a major role in the acceleration of wheat flowering
under long day photoperiod**

Andrew Chen, Chengxia Li, Wei Hu, Mei Yee Lau, Huiqiong Lin, Nathan C. Rockwell, Shelley
S. Martin, Judith A. Jernstedt, J. Clark Lagarias, and Jorge Dubcovsky*

correspondence to: jdubcovsky@ucdavis.edu or jclagarias@ucdavis.edu

This PDF file includes:

Materials and Methods
Supplementary Text
Figures S1 to S11
Tables S1 to S9

Supplementary Materials and Methods

Development of a *phyC* null mutant in wheat (*phyC^AB*)

We first obtained full length genomic sequences of the A (*PHYC^A*, KF859916) and B (*PHYC^B*, KF859917) homoeologs of *PHYC* from Kronos (Table S1) and developed genome specific primers to screen the Kronos TILLING population (1) (Table S2). We targeted the second exon, but since no premature stop codon or splice site mutations were identified for *PHYC^B* in this region, we targeted two additional regions in the first exon (Table S2). Using these primers, we identified 12 mutations in *PHYC^A* and 30 in *PHYC^B* that resulted either in truncations or amino acid changes (Table S3). Amino acid residues present only in wild-type *PHYC^B* and absent in *PHYC^A* and *PHYC* from other plant species are listed in Table S4.

To develop a tetraploid wheat mutant with no functional *PHYC* copies we selected one mutation each in the A and B genome copies of *PHYC*. For *PHYC^A*, we selected mutation T4-2327 (Table S3), which disrupts the donor splice site at the end of exon 2 and generates a premature stop codon. The protein encoded by this mutant is predicted to lack the last 179 amino acids of the C terminal region (Fig. 1A), which is critical for phytochrome dimerization (2). The truncated *PHYC^A* protein cannot form homodimers in yeast two-hybrid assays (Fig. S1A) and could not be detected in immunoblot analysis of the *phyC^AB* mutant indicating that the truncated *PHYC^A* protein is not stable (Fig. S1B).

For *PHYC^B*, we selected mutant T4-807 (Table S3), which encodes a protein with a C323Y substitution in the GAF domain (Fig. 1A). This Cys residue is required for binding the bilin chromophore. We confirmed experimentally that the C323Y *PHYC^B* mutant protein is not functional (Fig. S1). We cloned the *PHYC* N-terminal region encoding the conserved PAS-GAF-PHY photosensory core module from the wild type *PHYC^A* and *PHYC^B* homoeologs and from the T4-807 *phyC^B* mutant (C323Y). We used an *E. coli* system engineered for co-production of phytochromobilin (PΦB) chromophore to express these as holoproteins, which were purified and spectroscopically characterized as described before (3). When bound to PΦB, both wild-type holoproteins produced red and far-red absorption spectra characteristic of photo-active phytochromes (Fig S1C). By contrast, the C323Y protein product of the T4-807 mutant did not show any visible light absorption or photoactivity (Fig S1C right).

We backcrossed the *phyC^A* and *phyC^B* mutations to the non-mutagenized Kronos for two generations to reduce background mutations and intercrossed the BC₂ plants carrying individual *phyC^A* and *phyC^B* mutations. Plants homozygous for both mutations (henceforth *phyC^{AB}*) as well as those homozygous for either *phyC^A* or *phyC^B* single mutations were selected. We also obtained sibling lines lacking mutations in the *PHYC* genes to use as control. We determined flowering time of each of the four genotypes (8 plants per genotype) in Conviron[®] growth chambers under long-day (LD, 16 h light and 8 h dark) and short-day (SD, 8 h light/16 h dark) photoperiods (with one hour ramp at the beginning and end of the day) and temperatures of 22 °C during the day and 17 °C during the night (Fig. 1B-D).

Morphological characterization of the wheat *phyC^{AB}* mutant

Measurements were taken at physiological maturity from 8 plants per genotype (wild-type and *phyC^{AB}*). From each of these plants we determined the average number of nodes per stem and the average length of the first stem internode below the peduncle. Spike measurements were taken for three spikes from each of the eight plants, and within each spike from six spikelets collected in the middle of the spike. For each spikelet, we determined the length of the rachilla (distance between the base of the first and the base of the last floret), the glume, palea and lemma (without awns), and the awns from both glume and lemma (Fig. S3). Averages, standard errors of the means and statistical analyses for the morphological measurements are summarized in Table S6.

Effect of *phyC^{AB}* mutations on coleoptile length

Wheat seeds were sterilized with 30% bleach for 20 min, followed by thorough rinse with sterile ddH₂O. Seeds were then planted on MS salt media solidified with 0.8% phytagar, and imbibed at 4 °C in darkness for 4 days. Seeds were then exposed to white light for one day before being placed in the darkness or under blue (70 μmol m⁻² s⁻¹), red (50 μmol m⁻² s⁻¹), or far red (25-30 μmol m⁻² s⁻¹) light. Coleoptile lengths were measured from 7-days-old seedlings. The experiment was repeated three times (only two times for the far red light). Data from the three experiments were combined using experiments as blocks. ANOVAS were performed separately for each light condition. Normality of residuals was confirmed using the Shapiro-Wilk test and homogeneity of variances with Levene's test (SAS 9.2 (4)). Least-squares means were calculated to account for the different number of viable seedlings in the different experiments.

Scanning electron microscope (SEM) sample preparation

Spikelets were dissected at weekly intervals, fixed for a minimum of 24 hours in 2.5% formaldehyde + 2% glutaraldehyde in 0.1 M Sørensen's phosphate buffer (pH 7.0) (5), rinsed twice in the same buffer, and dehydrated through a graded ethanol series to absolute ethanol. Samples were critical-point dried in liquid CO₂ (tousimis ® 931 Series critical point drier), mounted on aluminum stubs, sputter-coated with gold (Bio-Rad SEM Coating System Model E5100), and examined with a Philips XL30 scanning electron microscope operating at 5KV. Images were recorded at slow scan 3 for high definition and saved as TIFF files (Fig. S3).

Split luciferase complementation assays

Split luciferase complementation assays (Fig. S4B) were performed to validate protein interactions identified by yeast-two-hybrid using published protocols (6). Bait vector pDuEx-Bait (C-terminal fragment of the *Renilla* luciferase protein, CLuc) and prey vector pDuEx-Prey (N-terminal fragment of the *Renilla* luciferase protein, NLuc) were used to generate the constructs used in the complementation assays. Rice protoplast isolation and transfection were conducted as published before (7).

Development of qRT-PCR systems

A qRT-PCR system previously developed for the barley homolog of *CCAI* (8) was used as a reference. Sequences for wheat homoeologs *CCAI-A* (IWGSC_chr7AL_ab_k71_contig_4552600) and *CCAI-B* (IWGSC_chr7BL_ab_k71_contig_6653841) were retrieved from the IWGSC (International Wheat Genome Sequencing Consortium, <http://www.wheatgenome.org/>) and were aligned to identify polymorphism between the A and B genome homoeologs. Primers were selected to avoid these polymorphisms and to amplify *CCAI* copies from both genomes. qRT-PCR systems for *PRR73*, *GI*, and *TOCI* were obtained from a previous study (9). Since B-genome homoeologs of these three genes are expressed at a higher level compared to the A-genome homoeologs (9), we used the B genome-specific primers for transcript quantification of these genes in Kronos. The qRT-PCR system for *FTI* was optimized and described in a previous study (10).

The A and B genome-specific sequences for *PPDI* (DQ885753 and DQ885757), *PRR59* (NCBI-WGS gi|457084550 and IWGSC_chr4BS_ab_k71_contig_4961544), *PRR95*

(IWGSC_chr5AL_ab_k95_contig_2092853 and IWGSC_chr5BL_ab_k71_contig_10800870), *COI* (IWGSC_chr7AS_ab_k71_contig_4256234 and IWGSC_chr7BS_ab_k71_ctg_3010418), and *CO2* (IWGSC_chr6AL_ab_k71_ctg_5775606 and IWGSC_chr6BL_ab_k71_ctg_4274671) were retrieved from NCBI and from the *Triticum aestivum* contig assembly at IWGSC. Primers designed in this study are listed in Table S5. To quantify transcript levels of both homoeologs simultaneously, qRT-PCR systems for these genes were designed in conserved regions of their respective A and B genome homoeologs. For *PHYC*, two additional pairs of qRT-PCR primers were developed to specifically amplify the A or the B genome copies of *PHYC* (Table S5). qRT-PCR systems for *PHYA* and *PHYB* were also designed to amplify both A and B genome copies simultaneously (Table S5).

Gene expression analysis

Total RNA was extracted from 50-100 mg of tissue using Spectrum™ Plant Total RNA kit (Sigma), following the manufacturer's instructions. RNA integrity was confirmed by the presence of distinct ribosomal bands on 0.8% agarose gels. First-strand cDNAs were synthesized from 2 µg of total RNA using the 'High Capacity Reverse Transcription' kit (Applied Biosystems) according to the manufacturer's recommendations. The resulting cDNA was diluted 1:5 in nuclease-free water and stored at -20°C. qRT-PCRs were performed using primers listed in Table S5 and in the previous section. Amplification was performed using 10 µL VeriQuest™ Fast SYBR GREEN® qPCR 2x Master Mix (Affymetrix) containing a Hot start Taq polymerase, 10 pmol of each primer, and 4 µL of the 1:5 diluted cDNA template in a final volume of 20 µL. Reaction conditions in a 7500 Fast Real-Time PCR machine (Applied Biosystems) were 50°C for 2 min, 90°C for 5 min, 35 cycles of two-step amplification including 95°C for 3 s and 60°C for 30 s.

To determine primer efficiency, a series of cDNA dilutions (1/4, 1/16, 1/64, 1/256 and non-template controls) were used as templates for amplification in qRT-PCR. Primer efficiencies are listed in Table S5. The resulting CT values (average of two technical replicates) were used to generate a standard curve from which the efficiencies were calculated. Dissociation analysis was performed at the end of each optimization run to confirm product specificity. PCR products were then sequenced to confirm sequence identity.

Circadian clock gene expression

To investigate the effects of *phyC^{AB}* on the circadian clock we tested the expression of several clock and clock-output genes. We entrained wild type Kronos and *phyC^{AB}* plants to 16 h light and 8 h dark (LD) for four weeks. We then collected leaf samples at 4 h intervals over a 24 h period, followed by either 48 h under continuous light and constant 20 °C (LL) or additional 24 h under continuous dark and constant 18 °C (DD). We then determined the transcript levels of circadian-clock genes *PRR73*, *PRR95*, *PRR59*, *PPD1*, *CCA1*, *TOC1*, *GI* and clock-output genes *CO1*, *CO2* and *FTI* (Figs. 3, and S8). All genes showed daily oscillations under LL confirming that they are under circadian regulation. Transcription profiles of these genes in Kronos were similar to those previously described for other wheat and barley varieties (8, 9).

Supplementary Figures

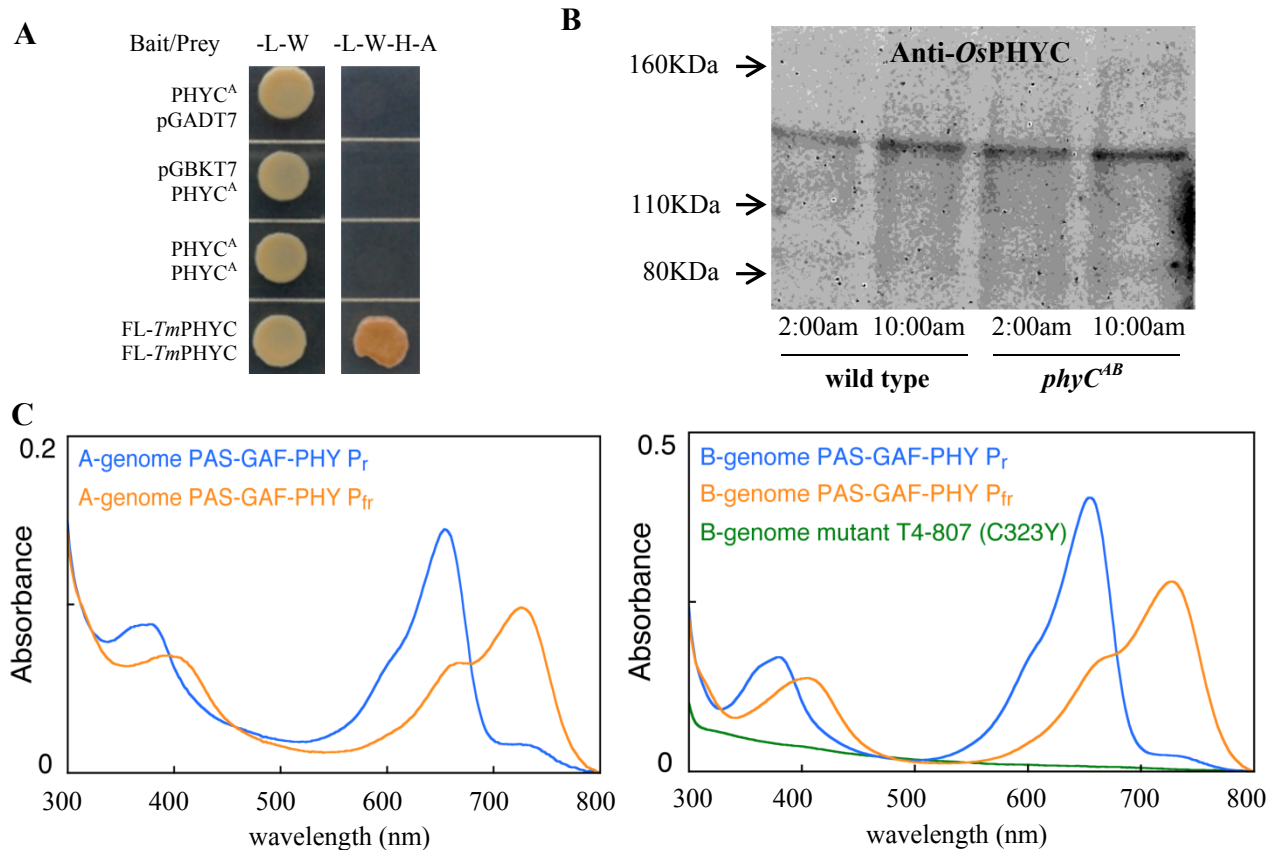


Fig. S1. Wild-type and mutant PHYC proteins. **(A)** The truncated PHYC^A is unable to form homodimers in yeast-two-hybrid assays, consistent with the known importance of the truncated region for phytochrome dimerization and function (2, 11). **(B)** Immunoblot analysis of soluble protein extracts from leaves of four-week-old wild type and *phyC^{AB}* grown under LD collected at 2:00 am (dark) and at 10:00 am (light). A single protein band corresponding to the full length PHYC protein (126 KDa) was detected both in Kronos (wild type) and in *phyC^{AB}*, indicating that both wild-type and mutant PHYC^B proteins are stable while the truncated PHYC^A protein (106 KDa) is not. **(C)** Absorbance spectra of recombinant photosensory domains of PHYC^A (left) and PHYC^B (right) are both photoactive, showing robust, reversible photoconversion between Pr (blue lines) and Pfr (orange lines) states. The *phyC^B* mutant T4-807=C323Y (green, right) is photoinactive since it lacks bound phytochromobilin chromophore.

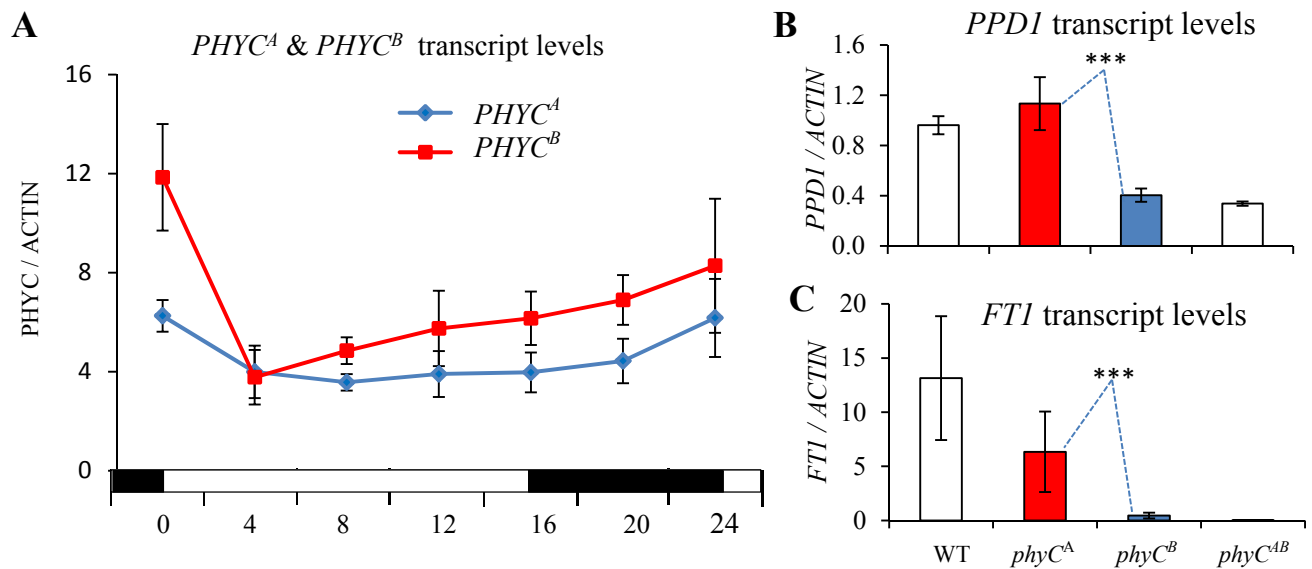


Fig. S2. Comparison between *PHYC^A* and *PHYC^B* homoeologs. **(A)** Transcript levels of *PHYC^A* and *PHYC^B* homoeologs in tetraploid wheat. Transcription profiles of *PHYC^A* (blue line) and *PHYC^B* (red line) homoeologs in wild-type Kronos. Plants grown under LD (16 h light, white bar and 8 h dark, black bar) were sampled at 4 h intervals over 24 h (third leaf of 5 different plants per time point). Although no significant differences were detected at individual time points, an overall ANOVA using time points as blocks showed significant differences between genotypes ($P=0.003$) and between light and dark time points ($P=0.0002$). **(B-C)** Transcript levels of **(B)** *PPD1* and **(C)** *FTI* in leaves of four-week-old wild type, *phyC^A* mutant (red bar), *phyC^B* mutant (blue bar), and *phyC^{AB}* (no active *PHYC*) mutants. The later flowering of *phyC^B* relative to *phyC^A* was associated with significant lower transcript levels of *PPD1* and *FTI* (***) ($P<0.0001$). Error bars represent standard errors of the mean from five **(A)** or eight **(B-C)** biological replicates. Transcript levels are expressed as fold-*ACTIN* using the delta CT method as described before (10) and in Supplementary Materials and Methods. Primers and primer efficiency are described in Table S5.

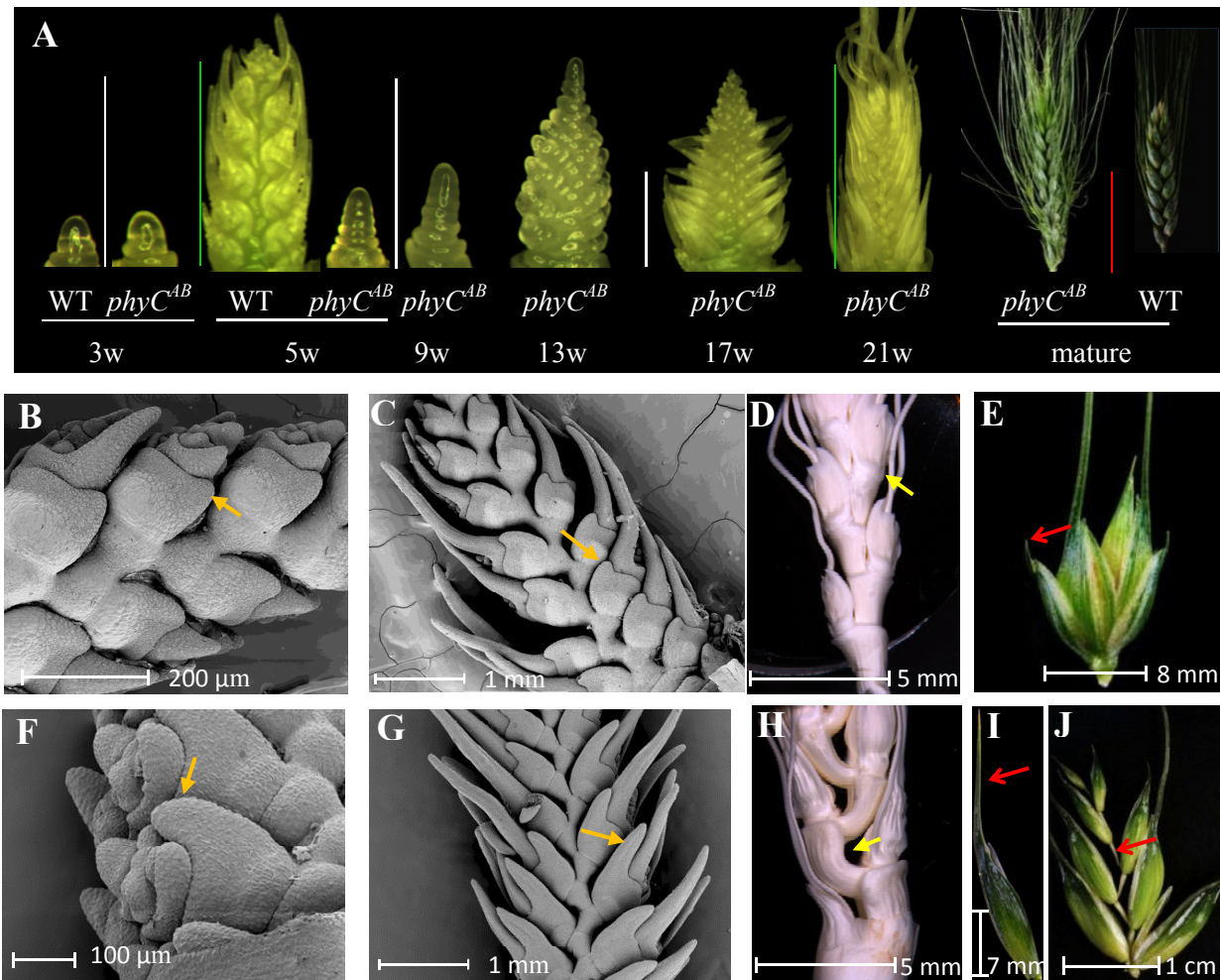


Fig. S3. Developmental differences between *phyC^{AB}* and wild-type (WT) sister lines grown under LD. (A) Comparison between WT and *phyC^{AB}* (w= weeks after germination). Note the faster development of WT and the more elongated glume awns in *phyC^{AB}*. Apex scales are indicated by 1 mm bars (white), except for WT-5w and *phyC^{AB}*-21w (1 cm green bar) and for mature spikes of WT and *phyC^{AB}* (5 cm red bar). (B-E) WT Kronos. (F-J) Wheat *phyC^{AB}* mutant. (B-C) Five-week-old wild type plants compared with (F-G) 13-week-old *phyC^{AB}* plants showing early elongation of the glume awns (orange arrows). (D and H) Spike's basal internodes (yellow arrows) are curved and longer in *phyC^{AB}* relative to WT. (E and I) Red arrows indicate the longer glume awn in *phyC^{AB}* relative to the WT. (J) Elongated rachilla in *phyC^{AB}*.

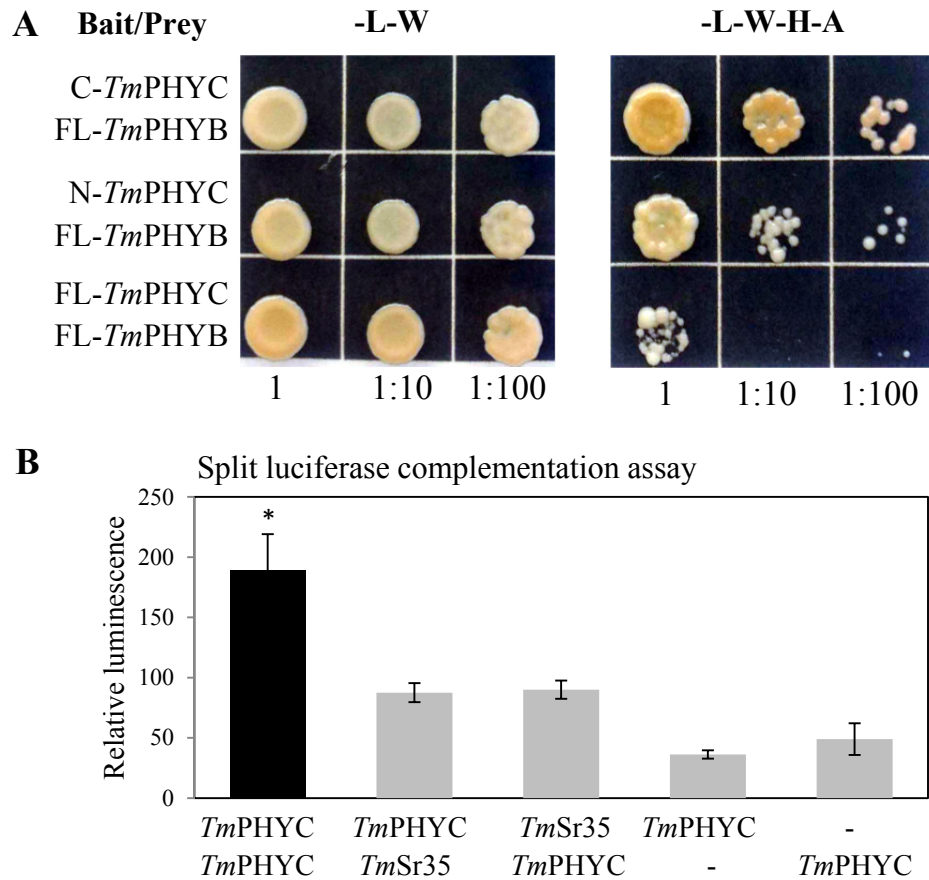


Fig. S4. PHYC protein interactions. **(A)** Protein interaction between *T. monococcum* PHYB and PHYC in yeast-two-hybrid assays. Synthetic dextrose minimal medium lacking Leu and Trp (-L-W) was used to select for yeast transformants containing both bait and prey vector (left panel). Interaction strength was tested on the same medium lacking Leu, Trp, His and Ade (-L-W-H-A, right panel). C and N indicate carboxyl and amino halves of the PHYC protein, respectively. FL indicates full length. Each panel consisted of three dilutions, from left to right, 1, 1:10, and 1:100. **(B)** Split luciferase complementation assay confirms the homo-dimerization of C-*Tm*PHYC in rice protoplasts. Luciferase activities were expressed as relative luminescence units. Bait vectors have the C-terminal fragment of the *Renilla* luciferase protein (CLuc) and prey vectors the N-terminal fragment of the same protein (NLuc). Negative controls include the LRR domain of the Sr35 protein (*Tm*Sr35) (12) fused to NLuc or CLuc, and co-transfected with PHYC as bait or prey. Additional negative controls include transfections with only bait or prey vector. *Tm*PHYC-*Tm*PHYC interactions were significantly stronger than all other pairwise comparisons (Tukey's Studentized Range Test $P < 0.05$).

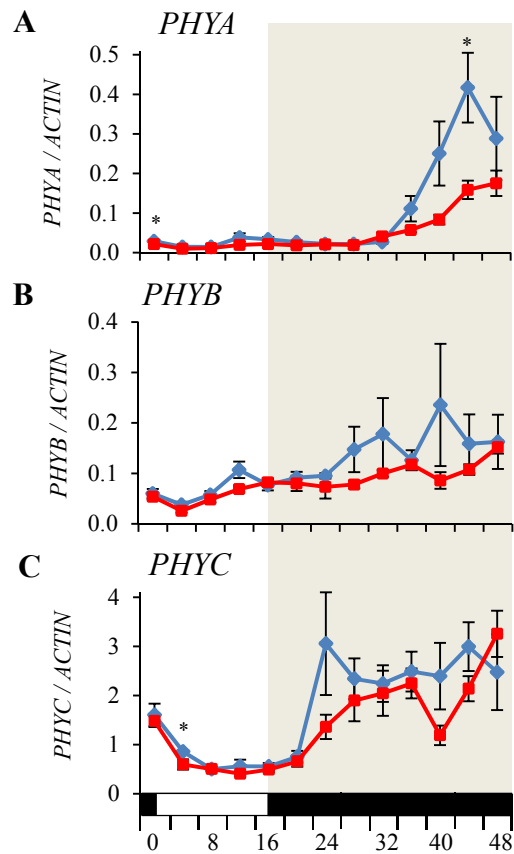


Fig. S5. Relative transcript levels of (A) *PHYA*, (B) *PHYB* and (C) *PHYC*. RNAs were extracted from leaves of 4-week-old wild-type (blue line) and *phyC^{AB}* mutant (red line) wheat plants grown under LD (16 h light and 8 h dark), followed by 24 h in continuous darkness (DD). Transcript levels of *PHYC* were approximately 10-fold higher than those of *PHYA* and *PHYB*. It is also interesting to point out that the strong upregulation of *PHYA* in the dark is significantly reduced in the *phyC^{AB}* mutant. Error bars are standard errors of the means from 5 biological replicates (plants). * = $P < 0.05$.

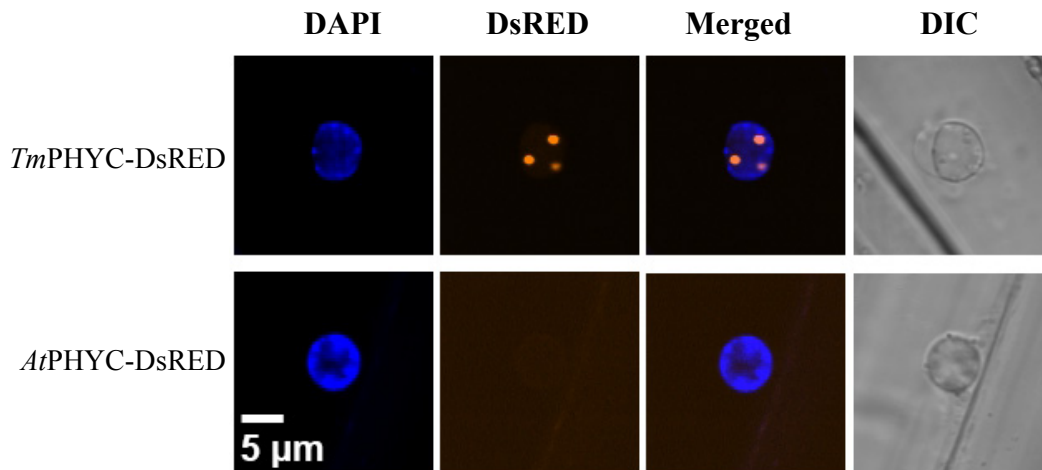


Fig. S6. Confocal fluorescence microscopy of wheat *TmPHYC-DsRED* and control Arabidopsis *AtPHYC-DsRED* constructs transformed into the Arabidopsis *phyABCDE* null mutant. After 1 d irradiation of 4-day-old seedlings with white light, *Triticum monococcum TmPHYC* localizes into the nucleus and forms few large nuclear bodies. No fluorescence is detected in the Arabidopsis *phyABCDE* plants transformed with *AtPHYC-DsRED*. DAPI (4',6-diamidino-2-phenylindole) was used to stain nuclei. Differential interference contrast (DIC) images are shown in the right panel.

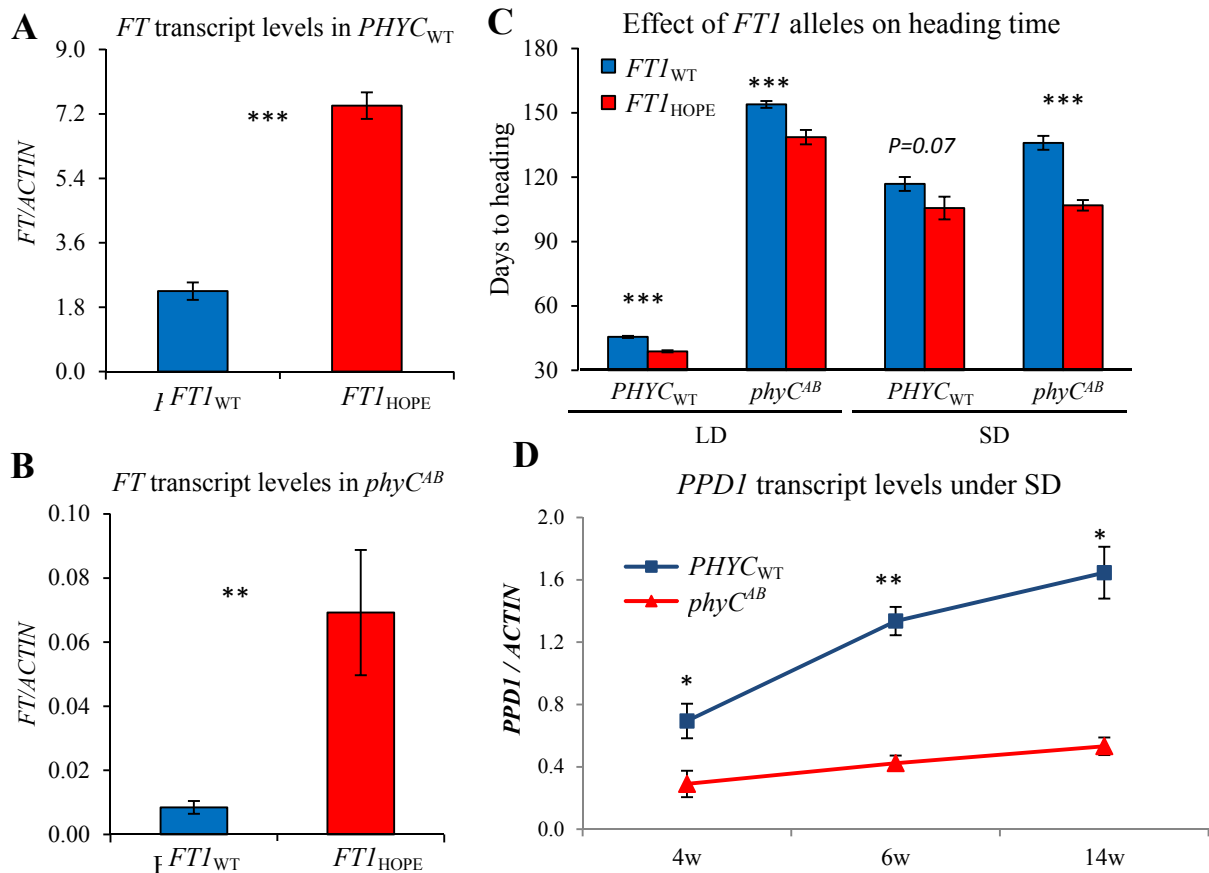


Fig. S7. Effect of different *FTI* alleles on PHYC regulation of flowering time. A natural allele of *FT* from the common wheat variety Hope (FTI_{HOPE}) was introgressed into Kronos by three backcrosses, and then combined with $phyC^A$ and $phyC^B$ mutations. This allele carries a repetitive element inserted in the *FTI* promoter and shows higher transcript levels than the *FTI* wild-type allele both under LD and SD (13, 14). **(A & B)** *FT* transcript levels in leaves of near isogenic plants differing in the FTI_{WT} and FTI_{HOPE} alleles. **(A)** Averages of eight $PHYC_{WT}$ Kronos plants (6-week-old). **(B)** Averages of twelve 17-week-old $phyC^{AB}$ plants. Note that FTI_{HOPE} transcript levels in $phyC^{AB}$ are 100-fold lower than those in wild-type Kronos, a result explaining their later flowering time. **(C)** Average heading times of 12 plants carrying either the FT_{WT} or the FTI_{HOPE} alleles. Plants carrying the FTI_{HOPE} allele flowered earlier than those carrying the FT_{WT} allele in both $phyC^{AB}$ and $PHYC_{WT}$ under both photoperiods. **(D)** Transcript levels of *PPD1* in $PHYC_{WT}$ (Kronos) and $phyC^{AB}$ mutant under SD conditions, 4, 6 and 14 weeks after sowing (for LD see Fig. 3 in main text). Error bars are standard errors of the means based on 8 different plants. All panels: * = $P < 0.05$, ** = $P < 0.01$, and *** = $P < 0.001$.

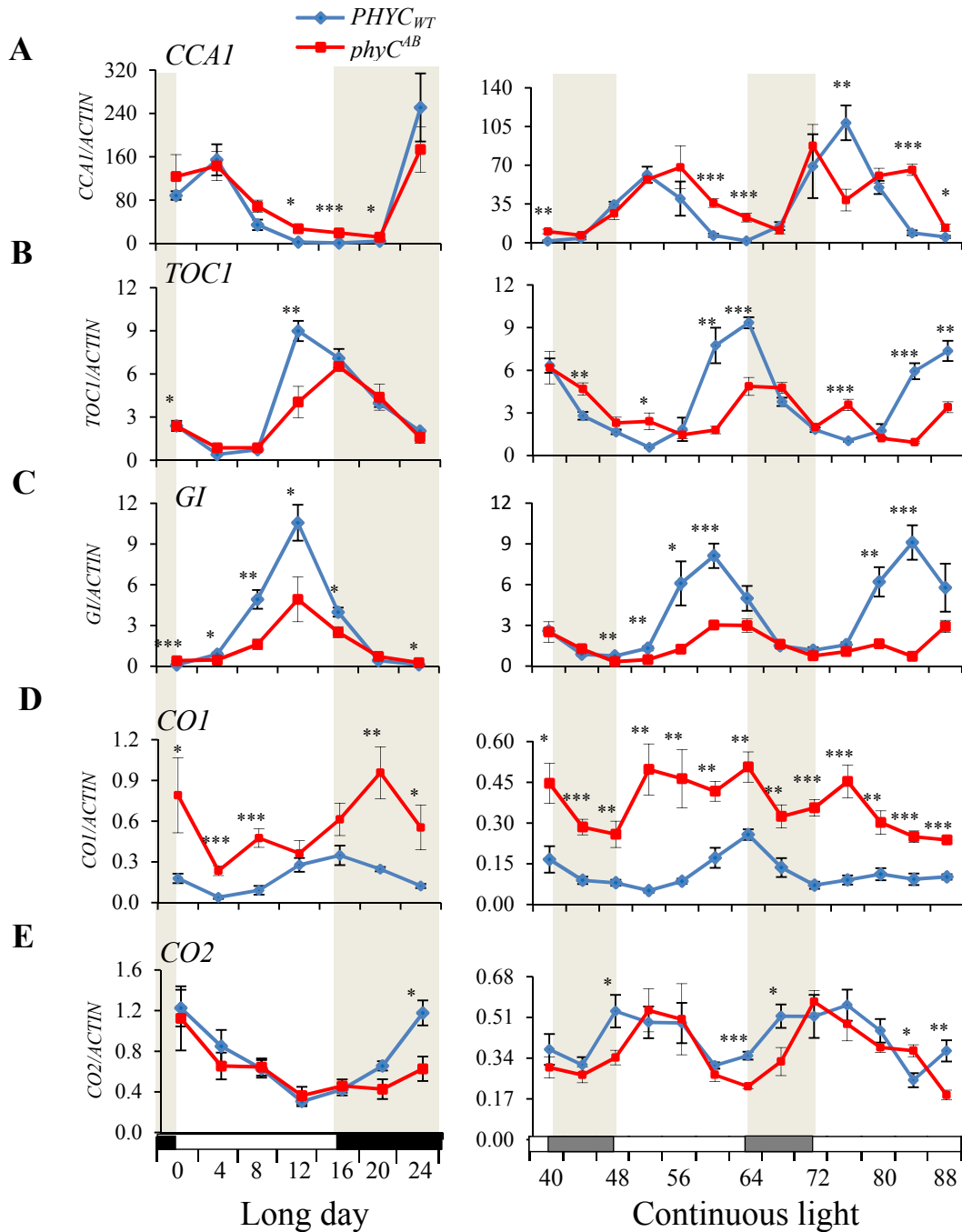


Fig. S8. Transcription profiles of (A-C) clock genes *CCA1*, *TOC1* and *GI*. (D-E) Clock-output genes *CO1* and *CO2* in Kronos wild type (blue lines) and *phyC^{AB}* (red lines). Left panels: plants grown under LDs (16 h light, white bar and 8 h dark, black bar) and sampled at 4 h intervals over 24 h. Right panels: plants were transferred to continuous light (LL) and sampled for another 48 h period, beginning at the start of the subjective night (grey bars). Asterisks indicate significant differences between wild-type and *phyC^{AB}* at each time point (* = $P < 0.05$, ** = $P < 0.01$, and *** = $P < 0.001$).

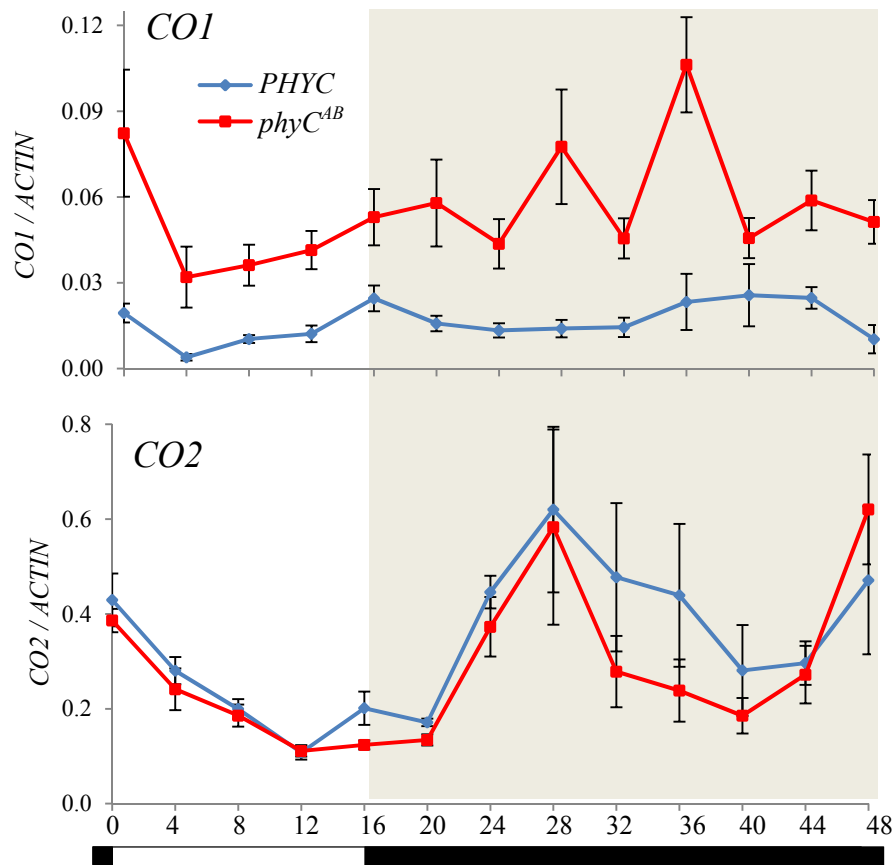


Fig. S9. *CO1* and *CO2* transcript levels in wheat wild type and *phyC^{AB}* mutant plants under continuous darkness. 4-week-old plants grown under long days were transferred to continuous darkness (DD). In wild-type Kronos, *CO2* transcript levels are significantly higher than those of *CO1*. The drastic transcriptional downregulation observed in *PPD1* and *FT1* under DD and under all light conditions in *phyC^{AB}* is not observed in *CO1* or *CO2*. *CO1* is upregulated in *phyC^{AB}* relative to wild type under LD, DD, and LL (see Fig. S8 for LL). *CO2* showed no significant differences in transcript levels between *phyC^{AB}* and wild type under DD but a significant shift in circadian oscillation was detected under LL (Fig. S8).

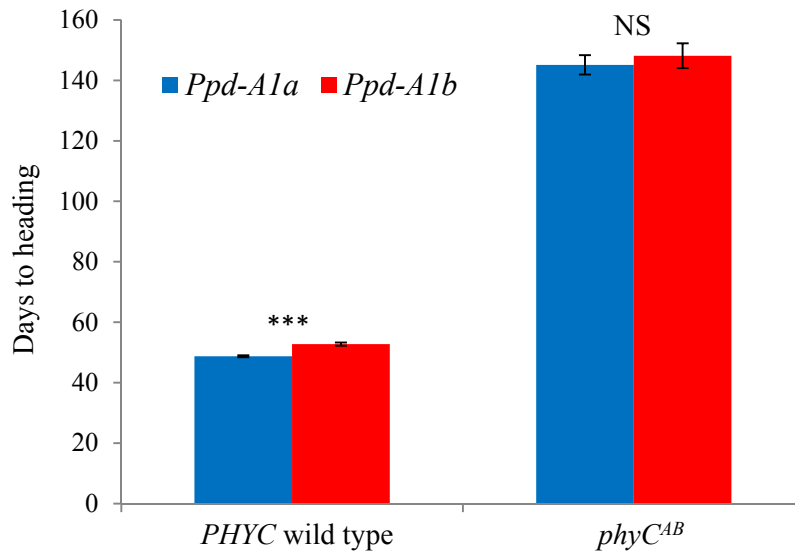


Fig. S10. Effect of *PPD-A1* alleles on heading time in Kronos and *phyC^{AB}* plants grown under LD. Previous studies have shown that the *Ppd-A1a* allele¹ has a 1,027 bp deletion in the promoter region that accelerates flowering under SD (30-40 days) relative to sibling lines carrying the *Ppd-A1b* allele (15). This experiment shows that these differences are greatly reduced or eliminated when plants are grown under LD. Under this condition, Kronos plants carrying the *Ppd-A1a* allele flowered only four days earlier than sibling lines carrying the *Ppd-A1b* allele ($P < 0.0001$). In the *phyC^{AB}* null mutant background, the differences between *Ppd-A1a* and *Ppd-A1b* alleles were only three days and were not significant ($P = 0.58$). The Kronos near isogenic line carrying the *Ppd-A1b* allele has been described before (14). This study confirms that the large differences in flowering time observed between Kronos plants carrying the wild-type *PHYC* and the mutant *phyC^{AB}* alleles (~100 d) are not affected by the *PPD-A1* alleles. Error bars are SE of the means based on seven to eight different plants. Plants were grown in a Conviron[®] growth chambers under LD (without ramp) and temperatures of 20 °C during the day and 17 °C during the night.

¹ The *Ppd-A1a* allele is frequently referred to in the wheat literature as “photoperiod insensitive” allele, because the accelerated flowering under SD reduces the differences between LD and SD relative to the “photoperiod sensitive” *Ppd-A1b* allele. However, Kronos plants carrying the *Ppd-A1a* allele flower more than 40 days earlier when grown under LD than when grown under SD, demonstrating that plants carrying the *Ppd-A1a* allele are still photoperiod sensitive.

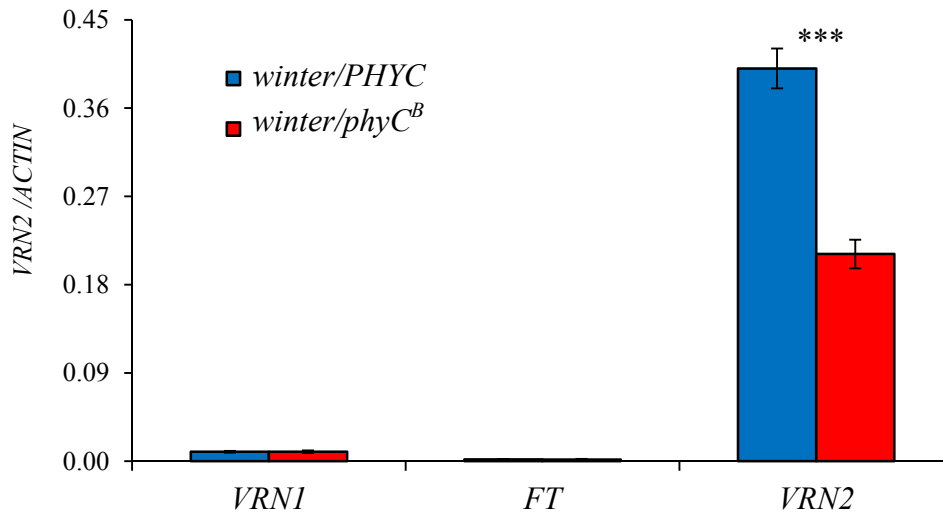


Fig. S11. Effect of *phyC^B* mutation on *VRN2* transcript levels. The effect of *PHYC* on the expression of *VRN2* was studied in a winter Kronos background because in the spring Kronos background the early expression of *VRN1* in the leaves results in the repression of *VRN2* transcription (10). For this study we introgressed the *phyC^B* mutation into a Kronos line with a winter growth habit caused by a non-functional mutation in *vrn-A1* (10). Because *PHYC* and *VRN1* are tightly linked (0.02 cM (16)), we were not able to separate the *vrn-A1* mutant from the functional *PHYC^A* allele, and therefore, could not combine the *phyC^{A/B}* mutation in a winter background. In spite of this limitation, we were able to detect a highly significant ($P < 0.0001$) reduction of *VRN2* transcript levels in the *phyC^B* mutant relative to a sister line carrying the functional *PHYC^B* allele. Both lines showed low *VRN1* and *FT1* transcript levels characteristic of winter lines. This result supports the hypothesis that the strong downregulation of *VRN2* reported in the *mvp* mutant (17) is caused by the deletion of *PHYC*. Error bars are standard errors of the mean of 11 independent plants (and 11 independent RNA extractions and cDNA syntheses per genotype).

Supplementary Tables

Table S1. Primer and PCR conditions used for sequencing the A and B genome copies of *PHYC* from Kronos. PCR was performed using Phusion *Taq* DNA polymerase (New England Biolabs) with 3% DMSO. Primers PHYC-SEQ-CF1 and PHYC-SEQ-CR2 amplified both *PHYC^A* and *PHYC^B* copies. These fragments were purified using a PCR purification kit (Qiagen) and were then cloned into a pGEM®-T-EASY vector (Promega). Colony PCR and sequencing was used to identify *PHYC^A* and *PHYC^B* copies.

Gene name	Target	Primer name	Primer sequence (5' to 3')	Product size (bp)	Ann. T (°C)
<i>PHYC^A</i>	Exon 1	<i>PHYC-5A_F3</i> <i>PHYC-5A_R5</i>	ACCGCTGCTGACCGTCGC TTCGCAAGCATAACCTGAGA	1249	60
<i>PHYC^A</i>	Exon 1	<i>PHYC-5A-SEQ-F1</i> <i>PHYC-5A-SEQ-R1</i>	GATGATATGTGATTGTGCTCCA CCTTGGATCTCCTTTGCT	730	64
<i>PHYC^A</i>	Exon 1-2	<i>PHYC-5A_F4</i> <i>PHYC-5A_R4</i>	GCTTCTGTGTGATATGCTCCTCA CTCTTCGGTTCCTGAAATAT	935	58
<i>PHYC^A</i>	Exon 3-4	<i>PHYC-5A-SEQ-F3</i> <i>PHYC-5A-SEQ-R3</i>	GCAAGGCATGTCTGTGAGCGAG CAATAGCCCTGGTTCACATCTC	867	66
<i>PHYC^B</i>	Exon 1	<i>PHYC-5B_F3</i> <i>PHYC-5B_R5</i>	ACTGCCGCTGCTGACCGTCGT TTCGCAAGCATAACCTGAGC	1244	60
<i>PHYC^B</i>	Exon 1	<i>PHYC-5B-SEQ-F1</i> <i>PHYC-5B-SEQ-R1</i>	GATGATATGTGATTGTGCTGCC CCTTGGATCTCCTTTGCC	730	66
<i>PHYC^B</i>	Exons 1-2	<i>PHYC-5B_F4</i> <i>PHYC-5B_R4</i>	CCTTCTATGTGATATGCTCCTCC CTCTTCGGTTCCTGAAATAC	933	58
<i>PHYC^B</i>	Exon 3-4	<i>PHYC-5B-SEQ-F3</i> <i>PHYC-5B-SEQ-R3</i>	GCAAGGCATGTCTCTGAGCGAA CAATGGCCCTGGTTCACATCTC	883	66
<i>PHYC^{A&B}</i>	Exons 1-3	<i>PHYC-SEQ-CF1</i> <i>PHYC-SEQ-CR2</i>	GGTGATTCTGTTGAAGTGGT CCGAGTAAATTGAAGCGTGC	1506 ^A 1498 ^B	64

Table S2. Sequences of genome-specific primer and PCR conditions for the detection of TILLING mutations. A region in exon 2 was targeted for the detection of mutations in *PHYC^A* and *PHYC^B*. For *PHYC^B*, two separate regions of exon 1 were also targeted and screened for additional mutations. All primer pairs amplified genome-specific PCR products that were confirmed by DNA sequencing.

Gene name	Target	Primer name	Primer sequence (5' to 3')	Product (bp)	Ann. T (°C)	Ext. time	5% DMSO	Enzyme
<i>PHYC^A</i>	Exon 2	<i>PHYC^A_F2</i> <i>PHYC^A_R2</i>	TGGTCCTTTTATGCTTTCCA TCTGCATCAGCACAGACACA	993	58*	1 min 30 s	No	-
<i>PHYC^B</i>	Exon 2	<i>PHYC^B_F2</i> <i>PHYC^B_R2</i>	TTGTGACACGTTGTGTTTCATT AGTTCTGCGTCAGCACACAC	946	59*	1 min 30 s	No	-
<i>PHYC^B</i>	Exon 1	<i>PHYC^{5B}_F3</i> <i>PHYC^{5B}_R5</i>	ACTGCCGCTGCTGACCGTCGT TTCGCAAGCATAACCTGAGC	1244	60*	1 min 30 s	Yes	-
<i>PHYC^B</i>	Exon 1	<i>PHYC^{5B}_F4</i> <i>PHYC^{5B}_R4</i>	CCTTCTATGTGATATGCTCCTCC CTCTTCGGTTCCTGAAATAC	933	58*	1 min 30 s	No	-
<i>PHYC^B</i> (CAPS)	T4-807	<i>PHYC^{5B}-807-</i> <i>CAPS-F1</i> <i>PHYC^{5B}-R5</i>	GGCATAACAAGTTCCACGAGGAT TTCGCAAGCATAACCTGAGC	442	60*	50 s	No	<i>BstEII</i>

*Touch-down protocol for PCR includes an additional 94 °C for 5 min, 12 cycles of initial touch-down, with a reduction of 0.5 °C per cycle (6 °C total from final annealing T), then followed by 40 cycles of 94 °C for 5 min, annealing temperature for 30 s and a final extension time of 7 min at 72 °C.

Table S3. Mutations detected in the A and B genome copies of *PHYC*. Mutations are organized by homoeolog and within homoeolog by targeted region. In the columns for nucleotide and amino acid changes, the first letter indicates the wild-type nucleotide/amino acid, the number its position, and the last letter the mutant nucleotide/amino acid. The nucleotide position is calculated from the 5' end of the forward primer whereas the amino acid position is calculated from the first methionine in the predicted protein sequence. High PSSM (>10) and low SIFT scores (<0.05) (18) predict mutations with severe effects on protein function. PSSM and SIFT scores are not reported for mutations that cause premature stop codons, altered splice sites or amino acid changes outside the conserved domains. Mutants analyzed in this study are indicated with an asterisk after the line name.

Gene (region)	Line	Nucleotide change	Amino acid change	PSSM	SIFT
<i>PHYC</i> ^A	T4-638	C136T	P710S	-	0.10
Exon 2	T4-2536	G150A	M714I	-	0.42
	T4-199	G223A	G739R	13.4	0.05
	T4-2729	G280A	V758I	3.6	0.38
	T4-471	G440A	G811E	-	0.02
	T4-1209	C617T	A870V	0.3	1.00
	T4-179	C692T	A895V	14.6	0.04
	T4-447	C743T	P912L	30.2	0.00
	T4-2190	C785T	S926F	17.5	0.00
	T4-437	G799A	E931K	12.2	0.04
	T4-2387	G877A	G957S	-6.5	1.00
	T4-2327*	G891A	Splice mutation	-	-
<i>PHYC</i> ^B	T4-2271	G147A	G729E	-	0.00
Exon 2	T4-1134	G158A	V733I	-	0.12
	T4-548	G187A	M742I	2.7	0.72
	T4-1294	C243T	P761L	14.1	0.08
	T4-128	C260T	P767S	31.2	0.00
	T4-584	G371A	V804I	-	-
	T4-1435	C378T	T806I	-	0.00

Continuation Table S3

Gene (region)	Line	Nucleotide change	Amino acid change	PSSM	SIFT
	T4-166	G413A	A818T	-	-
	T4-439	G459A	G833D	-	0.00
	T4-2258	C614T	L885F	6.9	0.08
	T4-2087	C645T	A895V	14.6	0.04
	T4-1212	G752A	E931K	12.2	0.04
<i>PHYC^B</i>	T4-719	C51T	R5W	-	0.02
Exon 1	T4-584	G79A	R14Q	-	0.01
F3 / R5	T4-2141	C190T	S51F	20.4	0.00
	T4-92	G195A	V53I	3.5	0.22
	T4-589	G229A	S64N	-	0.09
	T4-537	C282T	P82S	12.8	0.08
	T4-300	G483A	E149K	20.4	0.00
	T4-2080	C582T	L182F	-1.7	0.64
	T4-2238	C582T	L182F	-1.7	0.64
	T4-1416	G667A	R210K	6.6	0.26
	T4-778	C850T	A271V	21.6	0.00
	T4-807*	G1006A	C323Y	38	0.00
<i>PHYC^B</i>	T4-2097	C182T	T482I	24	0.00
Exon 1	T4-2412	G346A	E537K	16.1	0.05
F4 / R4	T4-423	G361A	D542N	20.7	0.01
	T4-2453	G502A	D589N	-	0.03
	T4-2502	C716T	T660M	-2.7	0.12
	T4-2534	G728A	G664E	28.6	0.00

Table S4. Non-conserved amino acids in wheat PHYC^B relative to other plant PHYC

Amino acid change ¹	BLOSUM62 ²	Domain	Conserved in
P91S	-1	PAS	Grasses ³
H536Q	0	PHY	Grasses & dicots ⁴
N593T	0	-	Grasses
R598G	-2	-	Grasses & dicots (R/K tolerated)
F732L	0	PAS	Grasses & dicots
T967A	0	-	Grasses s & dicots (T/S/C tolerated)

¹ The first letter indicates the conserved amino acid, the number the position in PHYC^B, and the last letter the amino acid in PHYC^B.

² The more negative BLOSUM62 values indicate changes with a higher probability of disrupting protein structure and/or function

³ Grasses compared include *Triticum aestivum*, *Hordeum vulgare*, *Oryza sativa*, *Sorghum bicolor*, and *Zea mays*.

⁴ Dicots compared include *Arabidopsis thaliana*, *Arabidopsis lyrata*, *Vitis vinifera*, *Cardamine nipponica*, and *Stellaria longipes*.

Table S5. Primer sequences for the SYBR GREEN qRT-PCR systems developed for *PPD1*, *PRR59*, *PRR95*, *CO1*, *CO2*, *PHYC*, *PHYC^A*, *PHYC^B*, *PHYA*, and *PHYB*.

Primer name	Primer sequences (5' to 3')	Primer efficiency (%)
<i>PPD1</i> -SYB-F3	CGGCATTCACGAGGTACAATAC	97.6
<i>PPD1</i> -SYB-R3	GAGCCTTGCTTCATCTGAGCG	
<i>PRR59</i> -SYB-F3	GCGTAACTTATGGCAACAT	95.4
<i>PRR59</i> -SYB-R3	CTGAGCATCACTTTTCCTC	
<i>PRR95</i> -SYB-F3	GACTATGGCAGATCAGAGGAC	95.4
<i>PRR95</i> -SYB-R3	TGAGCATCACCAGCGTTACC	
<i>CO1-AB-F3</i>	CACATCAGAGTGGTTATGC	96.0
<i>CO1-AB-R3</i>	GGACTGGACCGTATTGTC	
<i>CO2-AB-SYB-F4</i>	AAGGGTGTGAGTGTGTAG	98.5
<i>CO2AB-SYB-R5</i>	GATATGTCATTGCTGATGGAAG	
<i>PHYC</i> -QPCR-F3	CCTAGCAGACTACTTGGCA	98.0
<i>PHYC</i> -QPCR-R3	CTCATCGTCTTCACCAGC	
<i>PHYC^A</i> _SYB_F2	GCAAGGAACCGAAGAGCAG	98.5
<i>PHYC^A</i> _SYB_R2	CCTGTCAAATCTTGTGCTACG	
<i>PHYC^B</i> _SYB_F2	GCAAGGAACCGAAGAGCAA	97.0
<i>PHYC^B</i> _SYB_R2	CCCGTCAAATCTTGTGCTACC	
<i>PHYA</i> -QPCR-F3	CAGTGAAGTTCTCTCCTGTTG	95.3
<i>PHYA</i> -QPCR-R3	TCCCTGGTGCTTGATCC	
<i>PHYB</i> -QPCR-F3	GCTATGGGCAAATCATTAG	98.0
<i>PHYB</i> -QPCR-R2	TGGTCCTTTAGATTGCTCTGAC	

Table S6. Morphological traits measured three weeks after anthesis in *phyC^{AB}* and wild-type tetraploid wheat Kronos grown in chambers under LD photoperiod. Standard errors of the mean were calculated from 5 to 10 individual plants per genotype. For consistency, spikelet measurements including awn, rachilla, glume, lemma and palea were taken from spikelets located in middle of the spike (positions 4 to 8).

Trait	<i>PHYC-WT</i>	<i>phyC^{AB}</i>	<i>t</i> -TEST <i>P</i>
Number of nodes per stem	3.88 ± 0.08	4.09 ± 0.10	0.122
Length 1 st internode below peduncle (cm)	12.93 ± 0.37	9.75 ± 0.66	0.001*
Rachis length (cm)	6.27 ± 0.11	8.40 ± 0.36	<0.001*
Spike length (cm)	7.26 ± 0.14	9.48 ± 0.40	<0.001*
Number of spikelets per spike	16.86 ± 0.40	16.63 ± 0.85	0.818
Rachis internode length (cm)	0.32 ± 0.01	0.36 ± 0.01	0.015
Number of seeds per spike ²	30.3 ± 3.9	16.4 ± 2.34	0.008*
Number of floret per spikelet	4.29 ± 0.16	6.16 ± 0.31	<0.001*
Rachilla length (cm)	0.86 ± 0.05	1.73 ± 0.12	<0.001*
Glume length (cm)	0.81 ± 0.01	1.39 ± 0.03	<0.001*
Glume awn length (cm)	0.35 ± 0.02	4.76 ± 0.29	<0.001*
Lemma length (cm)	1.15 ± 0.02	1.40 ± 0.09	0.029*
Lemma awn length (cm)	12.83 ± 0.22	12.19 ± 0.79	0.474
Palea length (cm)	1.06 ± 0.01	1.05 ± 0.02	0.660

* Relative to wild-type Kronos, *phyC^{AB}* showed reduced internode elongation, reduced number of grains, increased number of florets per spikelet, and longer spikes, rachis, rachis internodes, rachilla, glume, glume awns and lemma.

² *phyC^{AB}* has the same number of spikelets per spike but reduced grain number per spike compared to the wild type, which indicates a reduced number of grains per spikelet. Since *phyC^{AB}* also has more florets per spikelet, this indicates that *phyC^{AB}* has a larger proportion of florets without viable grains. This phenotype is similar to a "constitutive shade plant" where shade signals inactivate phytochromes and increase floret mortality (19).

Table S7. Coleoptile lengths of *PHYC* wild-type and *phyC^{AB}* mutant seedlings in the dark and under continuous far red, red and blue light conditions (see Supplemental Material and Methods). Data represent adjusted least square means (LS-mean) from three experiments (FR only two experiments) \pm SE of the means. Experiments were included in the ANOVA as blocks.

Light	N	<i>PHYC</i>-WT (mm)	<i>phyC^{AB}</i> (mm)	<i>P</i> (WT vs. <i>phyC^{AB}</i>)	% change/Kronos
Dark	29	63.3 \pm 1.0	63.8 \pm 0.7	0.6965	NS
Far red	16	43.4 \pm 1.0	42.9 \pm 0.8	0.7258	NS
Red	38	35.8 \pm 0.7	39.5 \pm 0.6	0.0002	10.3%
Blue	38	29.2 \pm 0.6	30.2 \pm 0.4	0.1679	NS

Table S8. Primers used for yeast-two-hybrid constructs (restriction sites are underlined).

Gene	Primers	Primer Sequences (5' to 3')	Purpose
<i>PHYC</i> (full-length)	<i>TmPhyC</i> -Y2H-F1 <i>TmPhyC</i> -Y2H-R2	GGAATTCATATGTCGTCGTCGCGGTCCAAC TCCCCCGGGTCAGAAGTTACTCTTGCTCG	Bait & Prey
<i>N-PHYC</i>	<i>TmPhyC</i> -Y2H-F1 <i>TmPhyC</i> -Y2H-R1	GGAATTCATATGTCGTCGTCGCGGTCCAAC TCCCCCGGGAATTGACCTTGCATTGTTG	Bait & Prey
<i>C-PHYC</i>	<i>TmPhyC</i> -Y2H-F2 <i>TmPhyC</i> -Y2H-R2	GGAATTCATATGGTTGAAGCTCCATCTGATG TCCCCCGGGTCAGAAGTTACTCTTGCTCG	Bait & prey
<i>PHYB</i> (full-length)	<i>TmPhyB</i> -Y2H-F <i>TmPhyB</i> -Y2H-R	CCGAATTCATGGCCTCGGGAAGCCGCGC CCATCGATGCTCCGATCCCTACTTTCTG	Prey
<i>C-AtPHYC</i>	<i>AtPhyC</i> -Y2H-F1 <i>AtPhyC</i> -Y2H-R	GGAATTCATATGTTGTGTGTTATCGTGAATGAAATG TCCCCCGGGAATCAAGGAAATCTGTGAG	Bait & Prey
<i>phyC^d</i>	<i>phyC^A</i> -F <i>phyC^A</i> -R	GGGGACAAGTTTGTACAAAAAAGCTGCCACCATGTCGTCGTCGCGGTCCAAC GGGGACCACTTTGTACAAGAAAGCTGAACGGAAGTTACTCTTGCTCGTCG	Bait & Prey

Table S9. Primers used to generate binary constructs for Arabidopsis transformation (restriction sites are underlined).

Primer Name	Primer Sequences (5' to 3')	Name
PHYC-GW-F	GGGGACAAGTTTGTACAAAAAAGCTGCCACC <u>ATG</u> TCGTCGTCGCGGGTCCAAC	35S:: <i>Tm</i> PHYC-FLAG
PHYC-GW-R	GGGGACCACTTTGTACAAGAAAGCTGAACGGAAGTTACTCTTGCTCGTCG	
GATEWAY-F	GCGCTCTAGAACAAAGTTTGTACAAAAAAGC	35S:: <i>Tm</i> PHYC-FLAG
FLAG-R2	AATTGCGCGAGCTCTTACTTATCATCATCATCC	
PHYC- <i>Spe</i> I-F	GGACTAGTATGTCGTCGTCGCGGGTCCAAC	35S:: <i>Tm</i> PHYC-DsRED
PHYC- <i>Nde</i> I-R	GGAATTC <u>CATATG</u> GGAAGTTACTCTTGCTCGTCG	
DsRED- <i>Nde</i> I-F	GGAATTC <u>CATATG</u> GCGCGCTCCTCCAAGAAC	35S:: <i>Tm</i> PHYC-DsRED & 35S:: <i>At</i> PHYC-DsRED
DsRED-R	CCCGAGCTCCTACAGGAACAGGTGGTGGCG	
<i>At</i> PHYC- <i>Spe</i> I-F	GGACTAGTATGTCGTCGTCGCGGGTCCAAC	35S:: <i>At</i> PHYC-DsRED
<i>At</i> PHYC- <i>Nde</i> I-R	GGAATTC <u>CATATG</u> GGAAGTTACTCTTGCTCGTCG	

References Supplemental Materials

1. Uauy C, et al. (2009) A modified TILLING approach to detect induced mutations in tetraploid and hexaploid wheat *BMC Plant Biol* 9:115-128.
2. Matsushita T, Mochizuki N, Nagatani A (2003) Dimers of the N-terminal domain of phytochrome B are functional in the nucleus. *Nature* 424:571-574.
3. Rockwell NC, Martin SS, Feoktistova K, Lagarias JC (2011) Diverse two-cysteine photocycles in phytochromes and cyanobacteriochromes. *Proc Natl Acad Sci USA* 108:11854-11859.
4. SAS Institute (2011) SAS user's guide, version 9.2 (SAS Institute, Inc., Cary, NY).
5. Ruzin SE (1999) *Microtechnique and Microscopy* (Oxford University Press. New York.) p 322.
6. Fujikawa Y, Kato N (2007) Split luciferase complementation assay to study protein-protein interactions in Arabidopsis protoplasts. *Plant J* 52:185-195.
7. Bart R, Chern M, Park CJ, Bartley L, Ronald PC (2006) A novel system for gene silencing using siRNAs in rice leaf and stem-derived protoplasts. *Plant Methods* 2.
8. Campoli C, Shtaya M, Davis SJ, von Korff M (2012) Expression conservation within the circadian clock of a monocot: natural variation at barley *Ppd-H1* affects circadian expression of flowering time genes, but not clock orthologs. *BMC Plant Biol* 12:97.
9. Shaw LM, Turner AS, Laurie DA (2012) The impact of photoperiod insensitive *Ppd-1a* mutations on the photoperiod pathway across the three genomes of hexaploid wheat (*Triticum aestivum*). *Plant J* 71:71-84.
10. Chen A, Dubcovsky J (2012) Wheat TILLING mutants show that the vernalization gene *VRN1* down-regulates the flowering repressor *VRN2* in leaves but is not essential for flowering. *PLoS Genet* 8:e1003134.
11. Rockwell NC, Su YS, Lagarias JC (2006) Phytochrome structure and signaling mechanisms. *Annu Rev Plant Biol* 57:837-858.
12. Saintenac C, et al. (2013) Identification of wheat gene *Sr35* that confers resistance to Ug99 stem rust race group. *Science* 341:783-786.

13. Yan L, et al. (2006) The wheat and barley vernalization gene *VRN3* is an orthologue of *FT*. *Proc Natl Acad Sci USA* 103:19581-19586.
14. Pearce S, Vanzetti LS, Dubcovsky J (2013) Exogenous gibberellins induce wheat spike development under short days only in the presence of *VERNALIZATION 1*. *Plant Physiol* 163:1433–1445.
15. Wilhelm EP, Turner AS, Laurie DA (2009) Photoperiod insensitive *Ppd-A1a* mutations in tetraploid wheat (*Triticum durum* Desf.). *Theor Appl Genet* 118:285-294.
16. Yan L, et al. (2003) Positional cloning of wheat vernalization gene *VRN1*. *Proc Natl Acad Sci USA* 100:6263-6268.
17. Distelfeld A, Dubcovsky J (2010) Characterization of the *maintained vegetative phase* deletions from diploid wheat and their effect on *VRN2* and *FT* transcript levels. *Mol Genet Genomics* 283:223-232.
18. Ng PC, Henikoff S (2003) SIFT: Predicting amino acid changes that affect protein function. *Nucleic Acids Res* 31:3812-3814.
19. Ugarte CC, Trupkin SA, Ghiglione H, Slafer G, Casal JJ (2010) Low red/far-red ratios delay spike and stem growth in wheat. *J Exp Bot* 61:3151-3162.